Construction and Building Materials 328 (2022) 127090

Contents lists available at ScienceDirect

Construction and Building Materials

journal homepage: www.elsevier.com/locate/conbuildmat

Comparison of the condition of steel fiber-reinforced shotcrete with water-glass and alkali-free activators after more than 20 years of service in a subsea road tunnel

Cristobal Javier Manquehual [a,*], Pål Drevland Jakobsen [a], Karl Gunnar Holter [b], Klaartje De Weerdt [c], Tobias Danner [d], Amund Bruland [a]

[a] Department of Civil and Environmental Engineering, Norwegian University of Science and Technology (NTNU), Trondheim, Norway
[b] Norwegian Geotechnical Institute (NGI), Oslo, Norway
[c] Department of Structural Engineering, Norwegian University of Science and Technology (NTNU), Trondheim, Norway
[d] SINTEF Community, Architecture, Materials and Structures, Trondheim, Norway

ARTICLE INFO

Keywords:
XRD
μ-XRF
Sprayed concrete
Sulfur
Leaching
Chloride

ABSTRACT

The in-service condition of steel fiber-reinforced shotcrete installed more than 20 years ago as single-shell rock support lining in the Nordkapp subsea road tunnel was investigated. The novelty of this study is the comparison of shotcrete with water–glass and alkali-free activators in a saline groundwater environment. The lowest shotcrete density was obtained at joints between two adjacent shotcrete layers. In the case of alkali-free accelerator, ettringite enrichment was observed in these joints. Leaching appeared to be the main degradation mechanism in the outermost 10–15 cm towards the traffic room.

1. Introduction

Shotcrete is the standard method for permanent rock support in hard rock tunnels in Norway in combination of rock bolts [1]. The durability of shotcrete as a rock support element in these tunnels is crucial, as an inner lining of cast-in-place concrete is not usually installed, unless the geological conditions are extremely poor. A similar approach has been adopted in road tunnels constructed in Sweden and Finland [2].

The wet-mix shotcrete method was introduced for the first time in Norway in the early 1970s, but it took around a decade to be extensively used after it underwent several technological improvements. Among its innovations in the 1970s, one can highlight the shotcrete application using robots, the introduction of steel fibers in replacement of traditional wire meshes, the use of silica fume as an additive and the introduction of plasticizers in the mix [3]. Since the mid-1980 s, the steel fiber reinforced micro-silica wet-mix shotcrete method has completely dominated the shotcrete consumption in underground works in Norway [4]. Nowadays, the wet-mix spraying is the dominant method worldwide when it comes to spraying concrete [5].

A set accelerating agent is added to shotcrete in order to increase the hydration rate of the cement, achieving a higher early strength in the concrete sprayed and shortening its setting time [6]. Until mid-1990s, water soluble sodium silicate, also known as water–glass, was the most common accelerator in wet-mix shotcrete in Norway [7]. The fast hardening reaction of this accelerator is achieved by its content of silica reacting with the dissolved calcium ions (Ca^{+2}) in the fresh concrete, resulting in precipitation of calcium silicate hydrate compounds [8].

A non-alkaline shotcrete set accelerating admixture is defined according to NS-EN 934–5:2007 [9] by an alkali content (measured as Na_2O equivalent) less than 1% by mass of the admixture. Aluminum sulfate in liquid form is commonly used as the main component in alkali-free accelerators [6,10]. Ettringite is the main reaction product formed once the alkali-free accelerator is added [6].

In Norwegian subsea road tunnels, alkali-free accelerators were for the first time used in the Nordkapp tunnel. The Nordkapp tunnel was part of the Fatima project, a road connection between the island of Magerøya and the mainland of Norway. The location of the Nordkapp tunnel is shown in Fig. 1.

Nordkapp is a single-tube tunnel with two lanes, one in each direction. It has a total length of 6.8 km and a cross section of 44 m^2 [11]. The average daily traffic is 454 vehicles [12]. The tunnel construction started in May 1995 from its both ends. From the mainland side, it was

* Corresponding author.
E-mail address: cristobal.j.manquehual@ntnu.no (C. Javier Manquehual).

https://doi.org/10.1016/j.conbuildmat.2022.127090
Received 24 November 2021; Received in revised form 4 March 2022; Accepted 5 March 2022
Available online 9 March 2022

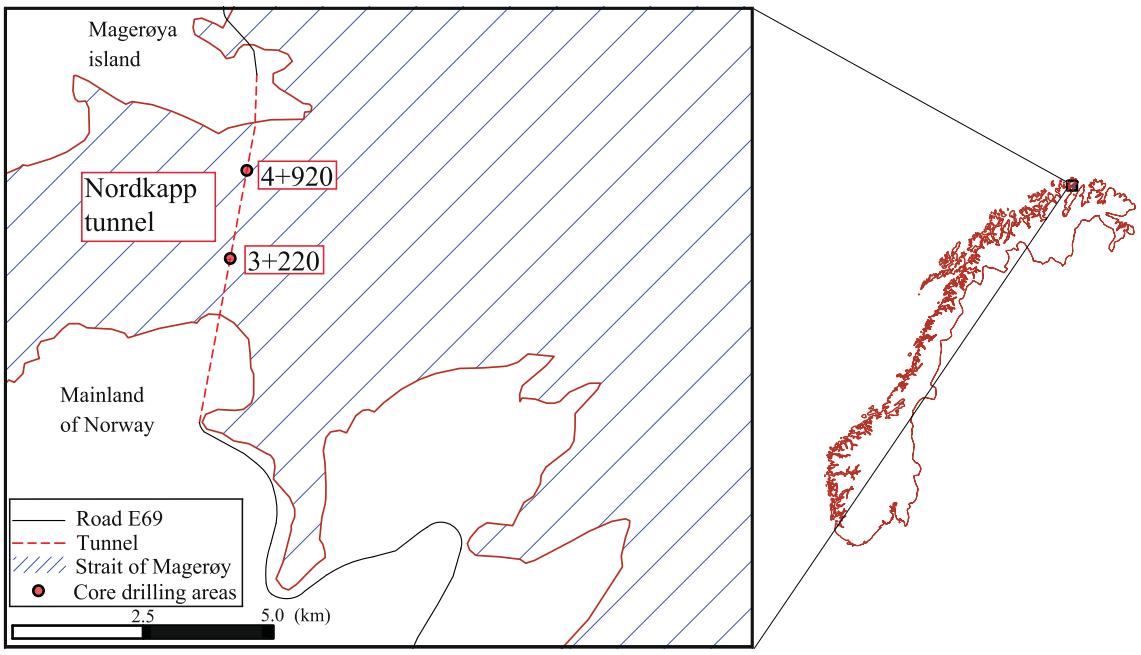

Fig. 1. Location of the Nordkapp tunnel and niches investigated in this study.

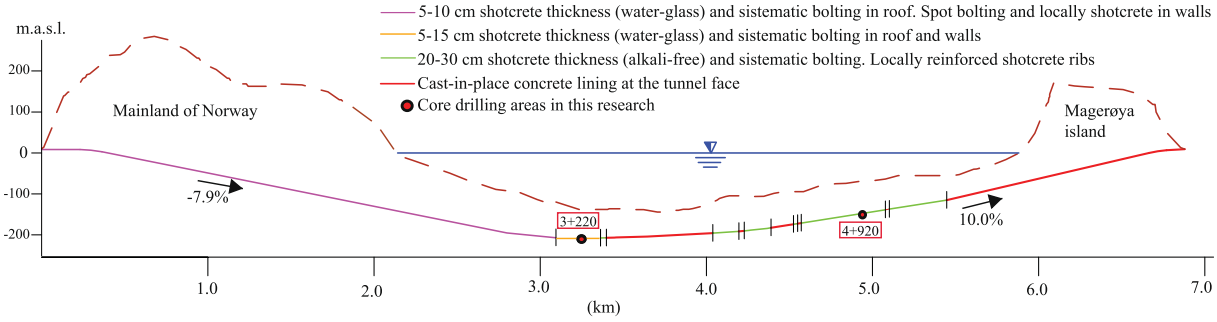

Fig. 2. Longitudinal profile of the Nordkapp tunnel with the final rock support distribution over chainage. (Modified from an unpublished as-built geological report prepared by the Norwegian Public Roads Administration).

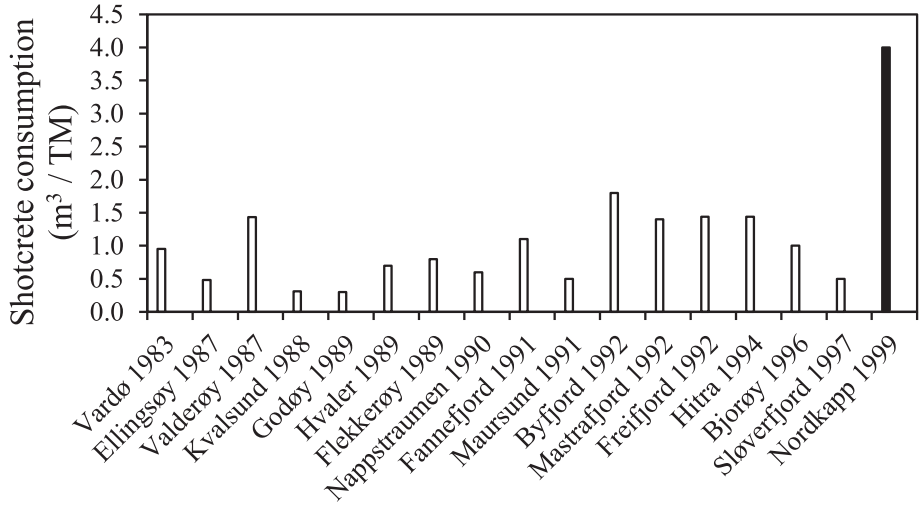

Fig. 3. Comparison of steel fiber-reinforced shotcrete consumption as rock support per tunnel meter (TM) in the Nordkapp tunnel with all the previous subsea road tunnels commissioned in Norway. Modified from [13].

Table 1
Wet-mix design in shotcrete with alkali-free accelerator used in the Nordkapp tunnel [11].

Aggregate 0–8 mm	1450	kg/m^3
Cement CEM I RR	520	kg/m^3
Silica fume	26	kg/m^3
Alkali-free liquid accelerator	33	kg/m^3
Plasticizer	5	kg/m^3
Superplasticizer	5	kg/m^3
Stabilisator	2.5	kg/m^3
Internal curing	5	kg/m^3
Steel fibers	40	kg/m^3
w/c	0.45	

experienced good rock mass conditions for almost 3400 m. Shotcrete with water–glass based accelerator was used in thicknesses between 5 and 10 cm in the first 3050 m and between 5 and 15 cm in the following 350 m (See Fig. 2). On the other hand, the excavation from the island side presented geological difficulties from the very beginning which required systematic cast-in-place concrete lining at the tunnel face [11]. These different geological conditions encountered from each tunnel face led to different excavation progresses. In September 1996, the excavation progress from the mainland had reached 3400 m, while that from the island side had only achieved 600 m. Since the mainland side started to cope with the same geological difficulties as the island side, cast-in-place concrete lining started to be used from both sides at the tunnel face. This prompted the search for alternatives in order to speed up the excavation rate. Several in-situ investigations trying to find the optimal composition of wet-mix shotcrete with alkali-free accelerator discovered that it was possible to spray concrete in thick layers thanks to the high early strength development achieved. Full scale application of alkali-free accelerator started in June 1997 from both sides, where the tunnel face from the mainland side had progressed 4050 m and the one from the island side had achieved 1200 m. This technological change in the shotcrete led to prevent the use of cast-in-place concrete lining in many stretches of poor rock mass conditions for the remaining 1550 m to be excavated [11]. The tunnel breakthrough occurred in January 1998, 4.5 km away from the mainland side. Fig. 2 shows the final rock support installed over chainage for the Nordkapp tunnel.

In Fig. 2, the tunnel stretch between 3.4 and 3.42 km also shows the application of shotcrete with alkali-free accelerator. This was probably an extra shotcrete layer applied after the tunnel breakthrough to reinforce the transition between cast-in-place concrete lining and shotcrete.

Fig. 3 compares the consumption of shotcrete in the Nordkapp tunnel with the consumption of other Norwegian subsea road tunnels previously commissioned.

A shotcrete mix design used in the Nordkapp tunnel is given in Table 1.

The wet-mix design of the shotcrete with the water–glass accelerator was probably the same as Table 1, except for the accelerator type. This statement is based on other Norwegian subsea road tunnels constructed in those years for the same owner as the Nordkapp tunnel [14]. However, an accelerator dose of 33 kg/m^3 (approximately 6.3% by weight of cement) per cubic meter of shotcrete seems a bit high for the common Norwegian practice in those years with the water–glass accelerator. For instance, the dose of water–glass accelerator in the shotcrete used in the Freifjord subsea tunnel, completed in 1992, was 5.2% by weight of cement. In the case of the Byfjord and Mastrafjord subsea tunnels, finished during the same year, the dose was 4.7% by weight of cement in

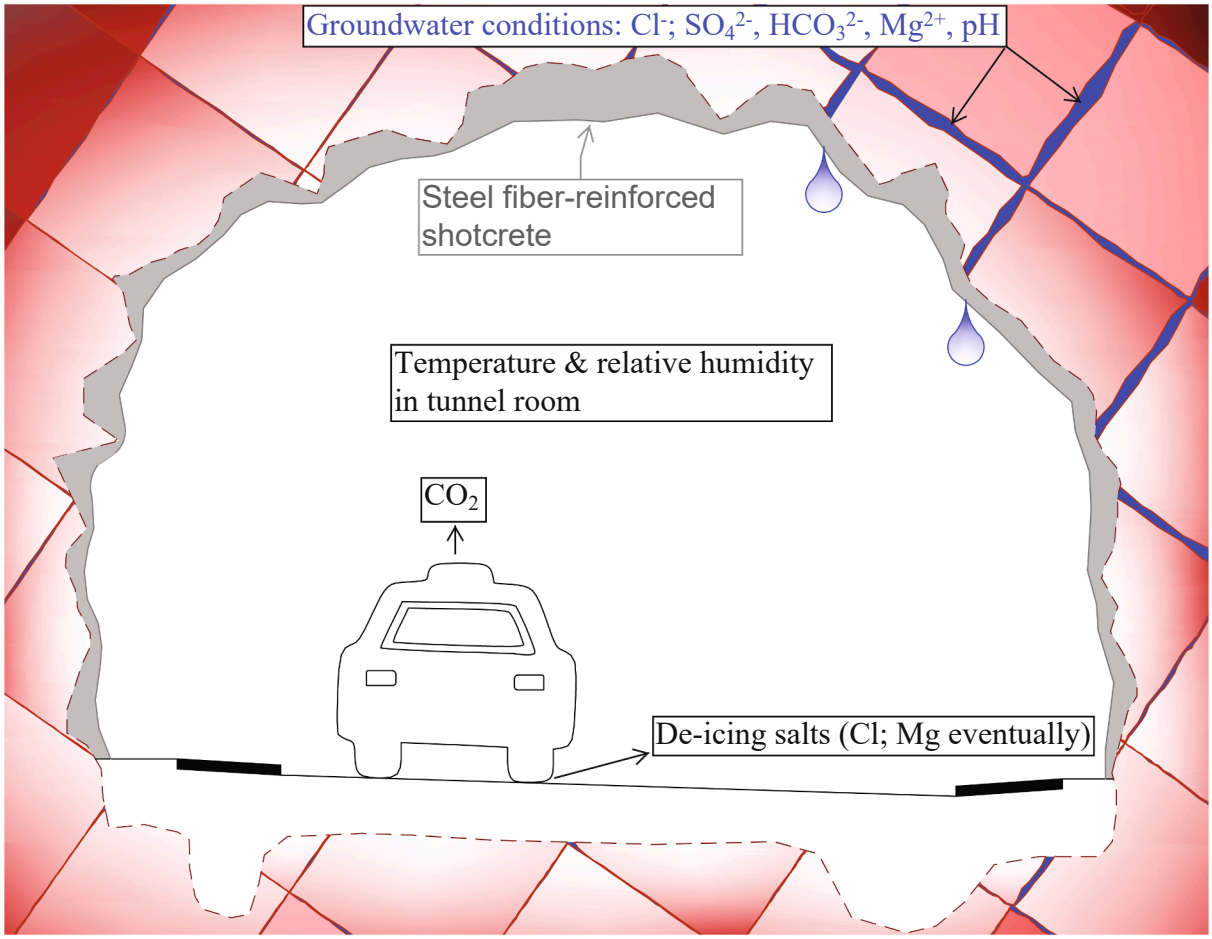

Fig. 4. Potential sources of aggressive elements for steel fiber-reinforced shotcrete installed in road tunnels without any inner lining.

Table 2
Extent of field work in each niche and some key features of their shotcrete and environmental conditions.

Zone	1	2
Tunnel	Nordkapp	Nordkapp
Chainage	3 + 220	4 + 920
Shotcrete core label	1–6	7–14
Total shotcrete thickness (cm)	9–11	25–32
Number of shotcrete layers	2	3 or 4
Type of accelerator	Water glass	alkali-free
Comments during drilling	1 core (No. 4) broke at the contact with the rock. 5 cores recovered rock.	2 cores (No. 8 and 9) broke at the contact with the rock. 2 cores (No. 7 and 10) broke at shotcrete joints. 4 cores (No. 11–14) recovered rock
Groundwater pH[(1)(2)]	7.3	7.8
Electrical conductivity of groundwater EC (mS/cm) [(1)(3)]	47.3 (saline)	48 (saline)
Estimated [Cl^-] (mg/l)[(4)]	15,460	15,688

(1) Dripping groundwater coming from the tunnel roof was collected after percolating the shotcrete layer.
(2) The measurement of pH was carried out by Laquatwin pH33, Horiba.
(3) The measurement of groundwater conductivity was carried out by Laquatwin-EC-33, Horiba.
(4) Estimation of the chloride concentration [Cl^-] (mmol/l) = 9.22·EC (mS/cm) [32].

both cases [14].

Steel fiber-reinforced shotcrete installed in tunnels as rock support is in direct contact with groundwater as long as the groundwater level is above the tunnel alignment [15]. Groundwater might percolate the shotcrete layer if there is a hydraulic gradient available from its contact with the rock to the traffic room. The magnitude of this gradient between both ends of the shotcrete layer in subsea tunnels depends on the height difference between the sea water level and the depth of the specific place in the tunnel, the permeability of the rock mass, the tunnel lining design and the atmospheric conditions in the traffic room. This gradient might be a relevant driving force for the movement of ions towards the traffic room in the shotcrete under study [16,17]. Then, shotcrete is susceptible to leaching [18], triggering eventually a reduction of mechanical strength, an increase in porosity [19] and a reduction of alkali metals (such as potassium) [20]. Leaching might be accentuated in tunnels which do not include an inner lining attached to the rock support, leaving the shotcrete layer alone to restrain percolation.

If groundwater holds sulfate ions, as may be the case in marine groundwater, it can trigger sulfate attack of the cement paste in the concrete. This attack promotes the formation of ettringite, gypsum and thaumasite [19]. In the latter compound, carbonate ions are needed in addition to sulfate ions for its formation. While the degradation mechanism of ettringite is related to expansion caused by the formation of voluminous water-rich ettringite crystals, the chemical deterioration causing the formation of thaumasite is related to a general disintegration of the cement paste due to the replacement of calcium-silicate-hydrate or in short C-S-H with thaumasite which has very poor cementing properties [19]. The formation of gypsum may lead to expansion and cracking in the cement paste [18]. Potentially, sulfate attack could also come from the constituents in the wet-mix. This might be the case for the aluminium sulfate compound in alkali-free accelerators, becoming shotcrete susceptible to internal sulphate attack [8,21]. Recent investigations in concrete have described the interaction between sulfate attack and leaching, indicating that the dissolution of hydrated cement phases caused by leaching facilitates the formation of secondary expansive minerals under an external source of sulfate [18,22]. Moreover, magnesium ions also available in seawater, might be aggressive for the concrete. As a result of magnesium attack, portlandite and C-S-H can be replaced by respectively brucite and M−S−H, which have inferior cementing properties [19].

Marine groundwater might also have chloride ions, which can attack the steel fibers. In ordinary Portland cement, free chlorides entering into the pore solution of the concrete can either react with hydration products, forming Friedel's salt for example, can be physically adsorbed on C-S-H hydrated cement due to its large surface area or remain as free chlorides in the pore solution [23,24].

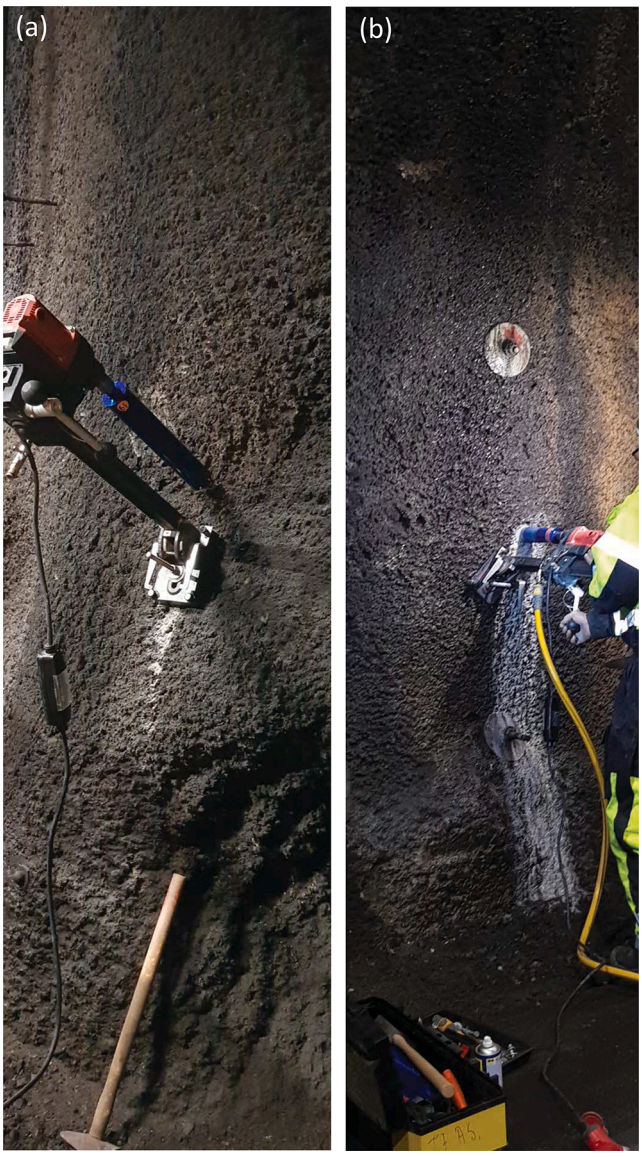

Fig. 5. Core drilling in: (a) Zone 1 located in the Nordkapp tunnel at chainage 3 + 220, and (b) zone 2 placed in the Nordkapp tunnel at chainage 4 + 920.

Table 3
Operating parameters for the μ-XRF surface mapping.

Parameter	Value
Step width	50 μm
Time per pixel	2 ms
Beam voltage	50 kV
Tube current	600 μA
Dead time	20%
chamber pressure	Vacuum, 20 mbar
Elemental filter	No filter

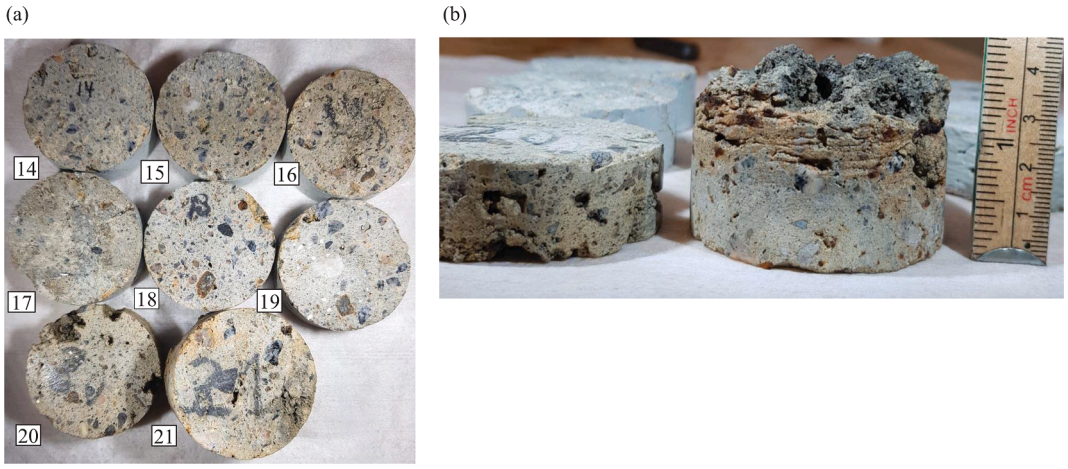

Fig. 6. Example of shotcrete samples for suction porosity test after the core has been sliced obtained from core 12 (zone 2 in Table 2).(a) Top view, and (b) in perspective.

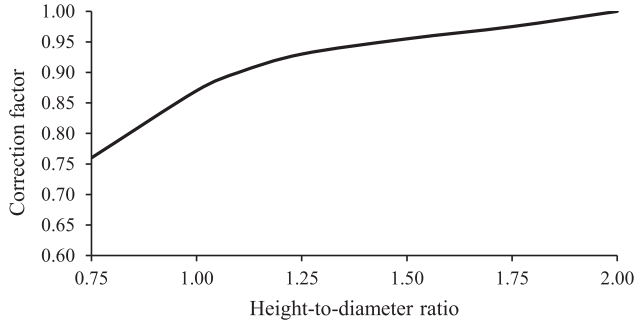

Fig. 7. Correction factor adopted for UCS test samples with a height-to diameter ratio lower than two, following Norwegian standard NS 3420:1986 [41].

Another consequence related to the absence of an inner lining in a tunnel is the exposure of shotcrete to the traffic environment. Carbon dioxide available in the air reacts through solution with the calcium rich phases such as portlandite and C-S-H, and results in the precipitation of calcite and alkali rich silica gel. This leads to a reduction in the pH of the pore solution [19]. The reduction of the pH favors the corrosion of steel fibers. Alike, the lack of an inner lining leaves the shotcrete layer exposed to de-icing salts, such as NaCl, $MgCl_2$ or $CaCl_2$, commonly used in roads located in cold winter climates. Its chloride content might also promote the corrosion of steel fibers.

Fig. 4 shows some environmental factors that might affect the durability of shotcrete installed in road tunnels.

The goal of the test program in the Nordkapp tunnel is to compare the in-service condition of shotcrete where water–glass and alkali-free accelerators were used in different stretches of this tunnel. Unlike the comparison of concrete with different accelerators in the laboratory [6,25,26], the comparison of shotcrete in the field incorporates construction variables such as the condition of joints between two adjacent shotcrete layers and the boundary between shotcrete and rock. Moreover, the environment of comparison is unique, combining the pollution of road tunnels with the saline groundwater of subsea tunnels. Finally, few other projects in the world provide the possibility to study shotcrete with alkali-free based accelerator installed more than 20 years ago.

After the introduction of alkali-free accelerators in shotcrete in the mid-1990s, its use has become widespread, and not only in Norway. Apart from the possibility to apply shotcrete in thicker layers, the literature highlights its low pH, reducing the risk of alkali-silica reaction in concrete [27]. In general, accelerators tend to reduce the long-term strength in comparison to concrete without this additive. In this regard, it is reported that concrete strength loss is minimal when alkali-free accelerator is used. In contrast, water–glass accelerator can reduce the long-term compressive strength between 20% and 50% [21,28,29]. Moreover, safer conditions for workers are claimed when using alkali-free accelerator instead of water–glass accelerator since the latter is highly caustic [10,27]. However, some authors have warned of the inconvenience of using alkali-free accelerators in concrete exposed to sulfur-rich environments [8,30,31].

In the tunnel under study, leaching was investigated by creating profiles along the cores of suction porosity, shotcrete density, Uniaxial Compressive Strength (UCS) and potassium content by Micro-x-ray fluorescence (μ-XRF). Eventual sulfur, chlorine and magnesium enrichments in specific areas of the different cores were also investigated by μ-XRF. The identification of deleterious minerals was undertaken by powder X-ray diffraction (XRD). In addition to concrete density, suction porosity and XRD tests, carbonation was investigated with Thymolphthalein pH indicator. Finally, iron mapping along the cores were undertaken through the μ-XRF technique to facilitate the identification of corroded and uncorroded steel fibers in the real images.

2. Experimental procedures in the field and laboratory

Since the tunnel was in operation when it was inspected, the cores were extracted from niches (emergency lay-bys in the tunnel). The inspection occurred on October 28, 2020. In the field, 14 shotcrete cores were drilled in total.

2.1. In the field

In order to apply different investigation techniques to the cores, the chosen places for core extraction are areas where a thick shotcrete layer was expected. Shotcrete where water–glass based accelerator was used in thicknesses larger than 10 cm is only found in the Nordkapp tunnel between chainages 3+050 and 3+400 (See Fig. 2). Then, one of the core drilling locations is at chainage 3+220 in the Nordkapp tunnel (see Figs. 1-2), called zone 1 in Table 2. The shotcrete surface on this zone appeared dry with dripping water nearby (See Fig. 5a).

The second niche chosen in the Nordkapp tunnel is at chainage 4 + 920. In this niche, alkali-free accelerator was used in the concrete sprayed. The shotcrete surface where the drillings occurred was wet and there was dripping water nearby (See Fig. 5b). This is zone 2 in Table 2.

The core drill machine used in both niches is the Hakken SPJ-122Hi with a diamond core bit of 62 mm as external diameter. The resulting shotcrete core diameter is 55.8 ± 0.2 mm. Table 2 summarizes the main characteristics of the shotcrete core extracted and the exposure

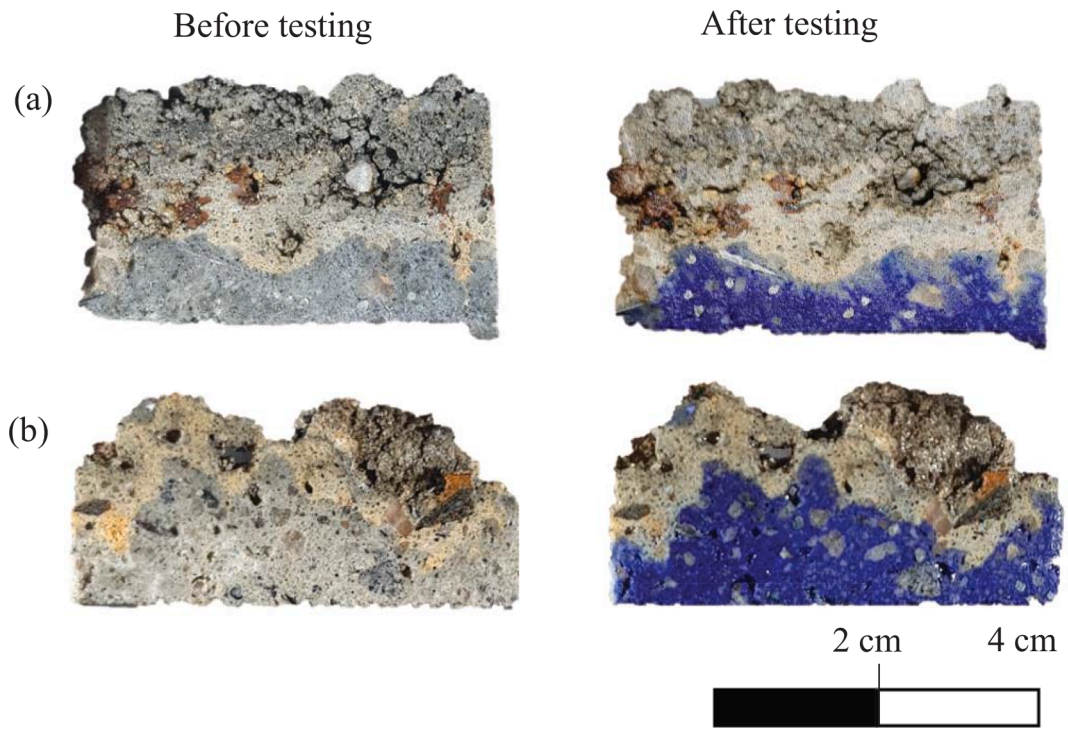

Fig. 8. Extent of carbonation in shotcrete samples exposed to the traffic room estimated by pH indicator Thymolphthalein: (a) core 5 (zone 1), and (b) core 9 (zone 2).

environment.

The electrical conductivity (EC) measured in Table 2 confirms the presence of saline groundwater in the two spots under study [33]. The estimated chloride concentrations, based on EC results, are coherent with water samples from other subsea tunnels in Norway [34]. In this reference, detail chemical analyses were undertaken in several Norwegian road tunnels. In particular, saline groundwater from subsea tunnels with similar chloride concentrations had sulfate ion content varying between 410 and 2,740 mg/l, magnesium ion content between 158 and 1420 mg/l and bicarbonates between 23 and 161 mg/l. According to the standard NS-EN 206:2013 [35], these ranges lie between slightly and moderately aggressive chemical environments for concrete.

At approximately 3:00 pm on the day of the inspection, the temperature and relative humidity in the tunnel at chainage 4+920 were 5° C and 69% respectively. As a reference, outside the tunnel, the temperature and relative humidity were −3° C and 90%. These atmospheric parameters were recorded with the instrument Reed R6020.

In the field, after core extraction, samples were marked, photographed, wrapped with stretch plastic film to prevent corrosion of steel fibers and further carbonation. On top of the plastic film, bubble wrap is used for transportation. The marking includes the number assigned to the core (see shotcrete core label in Table 2) and the orientation, being (T) the far-end towards the traffic room, and (R) the opposite end towards the rock.

2.2. In the laboratory

The procedures implemented for the different laboratory tests are described as follows.

2.2.1. pH indicator

Thymolphthalein was used to study the extent of the carbonation depth at the outermost part of the shotcrete cores exposed to the traffic room. This pH indicator sprayed on fresh surfaces of concrete gives a blueish color when the pH of the pore solution exceeds 10.5 [36]. Otherwise, it is colorless. This colorless area is related to the carbonation zone. In this research, the fresh shotcrete surface was achieved by splitting longitudinally the cores in halves with water-cooled saw just before spraying the pH indicator. The solution sprayed on the shotcrete surface consists of 1 g of Thymolphthalein dissolved in 30 ml of deionized water and 70 ml of ethanol.

The shotcrete cores 5 (zone 1) and 9 (zone 2) are analyzed with this pH indicator. The results are presented with images from the sprayed cores.

2.2.2. μ-XRF scanning

The 2D spatial distribution of sulfur, magnesium and chlorine along a shotcrete core is determined using μ-XRF analysis. The instrument used was an M4 Tornado from Bruker. The maps show the X-ray intensity related to the chosen chemical measured in counts per second (CPS) [37]. All maps are normalized individually to the highest intensity within the picture. This implies that this technique allows direct comparison in terms of intensities (element content) of two or more samples if scanned together. As no calibration was performed, the analysis does not provide absolute concentrations of a specific element.

Cores 2, 3 and 14 are fully split lengthwise in two halves to obtain a fresh, flat surfaces. They have a length of approx. 9 cm, 11 cm and 27 cm respectively. Therefore, the shotcrete samples for μ-XRF scanning are rectangles of 55.8 mm wide (diameter of the shotcrete core) by the length of the shotcrete core. Prior to the μ-XRF scanning, the relevant surface is dried by an air compressor. No polishing is undertaken on the flat surface to be scanned. Thereafter, the whole sample is inserted in the chamber of the M4 Tornado. However, the scanning area of the instrument is only a rectangle of 160 mm × 190 mm. This size allows to compare two different shotcrete samples put in parallel. However, longitudinally the scanning of core 14 is trimmed to the scan range of the instrument.

Apart from detecting the distribution of potential aggressive elements along the shotcrete cores, iron is also mapped along the cores to facilitate the identification of steel fibers, with or without signs of corrosion.

Finally, leaching was also studied with the M4 Tornado. A decrease

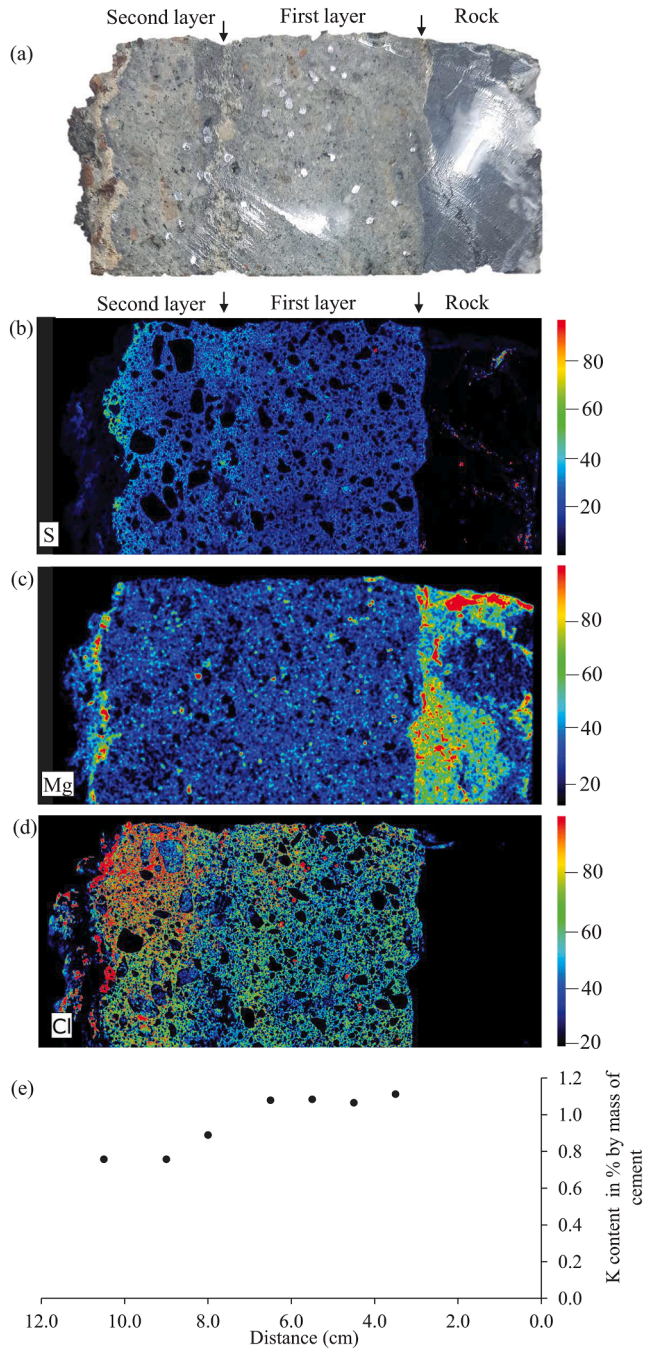

Fig. 9. μ-XRF analysis in core 3 (See Table 2): (a) One half of the shotcrete core split lengthwise, (b) sulfur mapping along the core, (c) magnesium mapping along the core, (d) chlorine mapping along the core and (e) profile of potassium content along the core in mass percent of cement.

in potassium content in the pore solution towards the traffic room is an indication of this deterioration process. The M4 Tornado software allows distinguishing different phases (e.g., aggregate and cement paste) by dividing the whole scanned area into smaller areas of similar chemical composition. Once a phase is defined, it is possible to retrieve its spectra. In particular, calcium is adopted to obtain the cement paste phase in a concrete sample [20]. By choosing this element to distinguish the cement paste from the aggregates, the potassium content in the cement paste is determined semi-quantitatively with the software. A profile of potassium content present in the cement paste is achieved after a discretization of the whole surface area of the shotcrete sample into smaller mapping areas, retrieving in each of these areas the corresponding spectra of the cement paste. From these spectra, averaged potassium content is obtained for each smaller mapping area [38]. From the same spectra, relative concentrations of chlorine by mass of cement are also given.

The M4 Tornado is equipped with a silver X-ray tube and two SDD detectors. The X-ray beam is focused by polycapillary lenses to a spot size of 20 μm. The operating parameters used for surface mapping are given in Table 3:

In the case of mapping smaller areas for spectra extraction, the operating parameters are the same except from the step width of 25 μm and the time per pixel of 5 ms to increase the signal statistics.

2.2.3. XRD

X-ray powder diffraction analysis was used qualitatively to identify the different minerals present in some shotcrete samples. Mineral phases were identified with the PDF-4 + 2021 database from the International Centre for Diffraction data. In addition, phase quantification via Rietveld analysis was performed with the software Topas from Bruker. Among the minerals to be searched are calcite as an indication of carbonation, thaumasite, gypsum and ettringite as an indication of sulfate attack, along with brucite as an indication of magnesium attack. The instrument used is the D8 Advance from Bruker. After slicing the core to obtain bulk shotcrete samples for XRD test, the samples are crushed in a fly press rock crusher to about 2 mm. At this stage, samples are split in groups of about 25 g. The crushing continues in a disc mill to reach a particle size of about 50 μm. Samples are then crushed in a McCrone micronizing mill to about 10 μm in ethanol. The following operating parameters are used: step size 0.01°, time per step 0.6 s, rotation 60 rpm, radiation 1.79 Å (Co-Kα) with a generator voltage and current of 40 kV and 40 mA respectively.

2.2.4. Suction porosity

According to the SINTEF procedure KS 70110 [39], suction porosity in a concrete sample is estimated as follows:.

1. Drying at 105 °C until constant weight loss (0.01% within an hour).
2. Cooling for two hours at room temperature before measuring the weight (W_1).
3. Immersion in water for seven days.
4. Measuring the weight of the sample (W_2).
5. Measuring the apparent weight of the sample immersed in water (W_2^*).

The samples for this test are disc-shaped, where the sample diameter coincides with the core diameter. When it comes to disc thickness, the shotcrete cores used for suction porosity analysis were sliced each 20 mm in the longitudinal direction following [39]. The sample size exception is for the ones exposed to the traffic room with an uneven surface on one side. These latter samples have in all cases a larger volume than the disc-shaped ones.

Eq. (1) describes the determination of suction porosity p_s as follows:.

$$p_s = \frac{W_2 - W_1}{W_2 - W_2^*} \tag{1}$$

The balance used in the lab is the Mettler PC4400 with a fine weighing range of 400 g and a readability of 0.01 g.

In total, 22 suction porosity tests are executed from the cores 1 and 2 (zone 1), and cores 7 and 12 (zone 2). One has to bear in mind that, in the longitudinal direction, approximately 5 mm of sample material are lost each time the core is sliced (thickness of the saw blade).

Fig. 6 shows samples 14–21 in core 12 before being tested.

2.2.5. Uniaxial compressive strength with axial strain measurements

In total, 14 UCS tests are executed in the Triaxial Testing Systems GCTS RTRX-140CL9. In order to get a profile of UCS test results in a

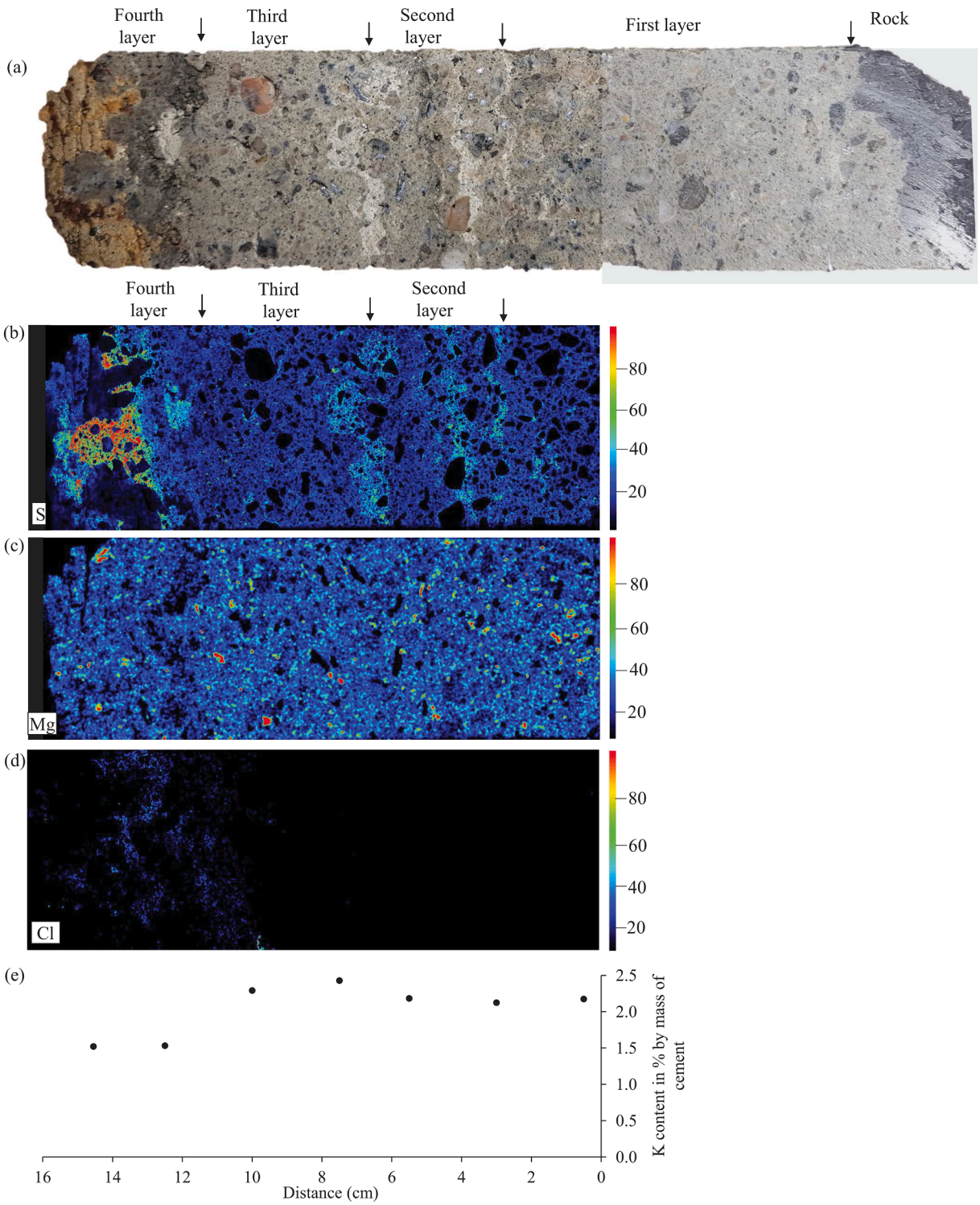

Fig. 10. μ-XRF analysis in core 14: (a) One half of the shotcrete core split lengthwise, (b) sulfur mapping along the core, (c) magnesium mapping along the core, (d) chlorine mapping along the core and (e) profile of potassium content along the core in mass percent of cement.

single shotcrete core, shorter samples were adopted. While five sample tests are undertaken for a height-to-diameter ratio (h/D) of two, fulfilling standard NS-EN 12390–1:2012 [40], the remaining nine samples have a nominal height-to-diameter ratio of one. In order to homologate all the UCS test results, a correction factor was applied for those shorter samples as shown in Fig. 7:

The diameter of the samples for the UCS test is fixed by the drilled core diameter. Vertical strain measurements are included in the execution of the UCS tests to visualize eventually differences in the post-peak behavior between different samples. For this reason, the loading procedure chosen is strain controlled instead of the usual constant load rate. According to standard NS-EN 12390–3:2019 [42], the latter rate for the compressive strength of hardened concrete should be 0.6 ± 0.2 MPa/s. By an adjustable strain rate applied for each sample calibrated with low magnitude stress cycles, most of the tests are within the load rate range stated in standard [42] before the samples reach the peak

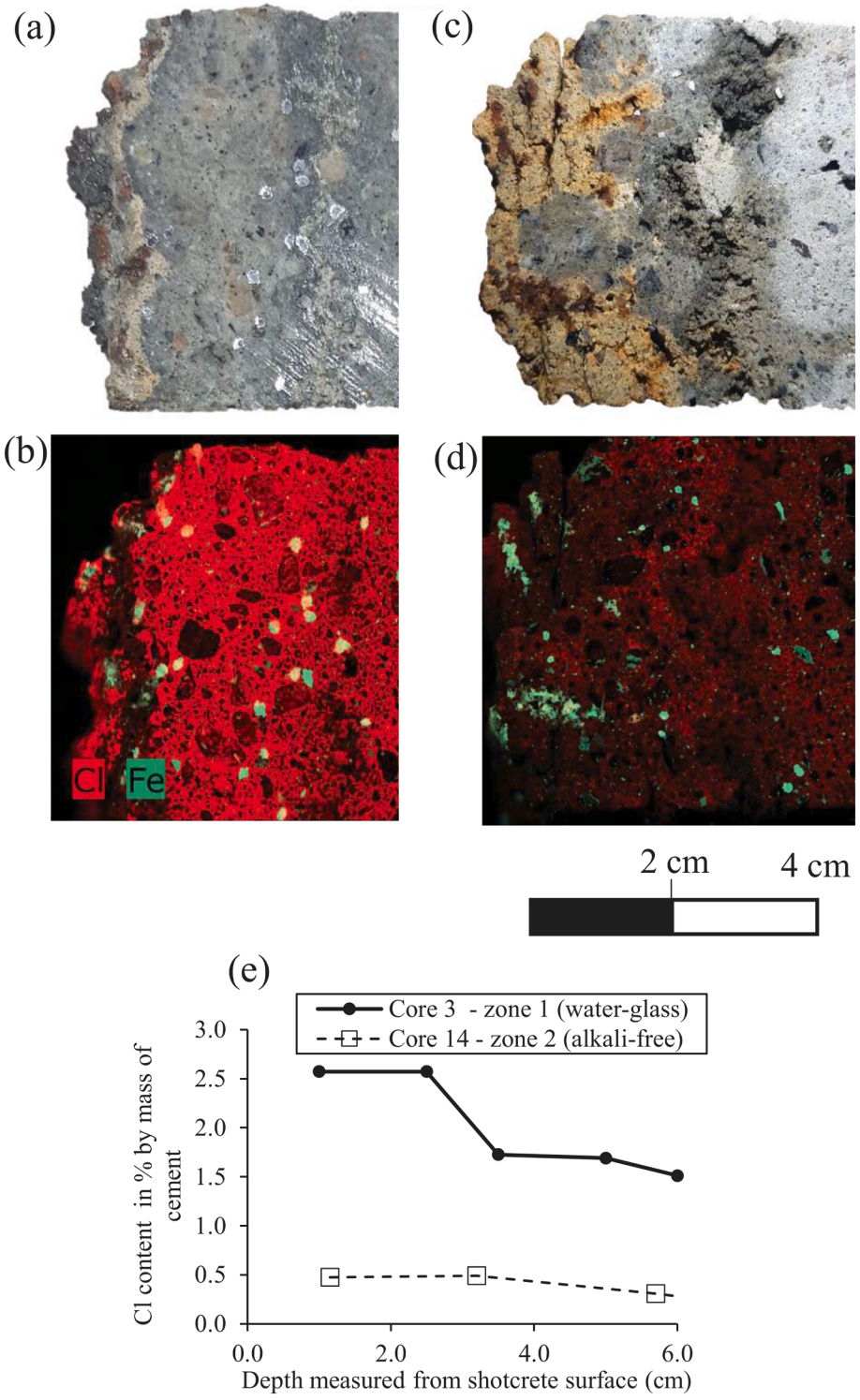

Fig. 11. Closeup for cores 3 and 14 near the traffic room. (a) Core 3 image near the traffic room, (b) chlorine and iron mappings in core 3, (c) core 14 image near the traffic room, (d) chlorine and iron mappings in core 14, and (e) profiles of Cl concentration near the shotcrete surface in both cores.

load. The type of sensor used for the vertical strain measurement is the LVDT SR-DF-C375-100 with a theoretical accuracy of 0.001 mm. Any correction factor was applied to the stress–strain curve results.

The shotcrete samples were sliced, ground and immersed in water for seven days before testing.

2.2.6. Shotcrete density

The bulk density of shotcrete samples described in this research is connected to the weight gained by the samples after they have been immersed in water for at least seven days (W_2), following the SINTEF procedure [39]. The balance used for the weight measurement is the same as in the suction porosity test.

In the case of samples used for the suction porosity test, their volume is determined by the buoyancy method as described in Eq. (2).

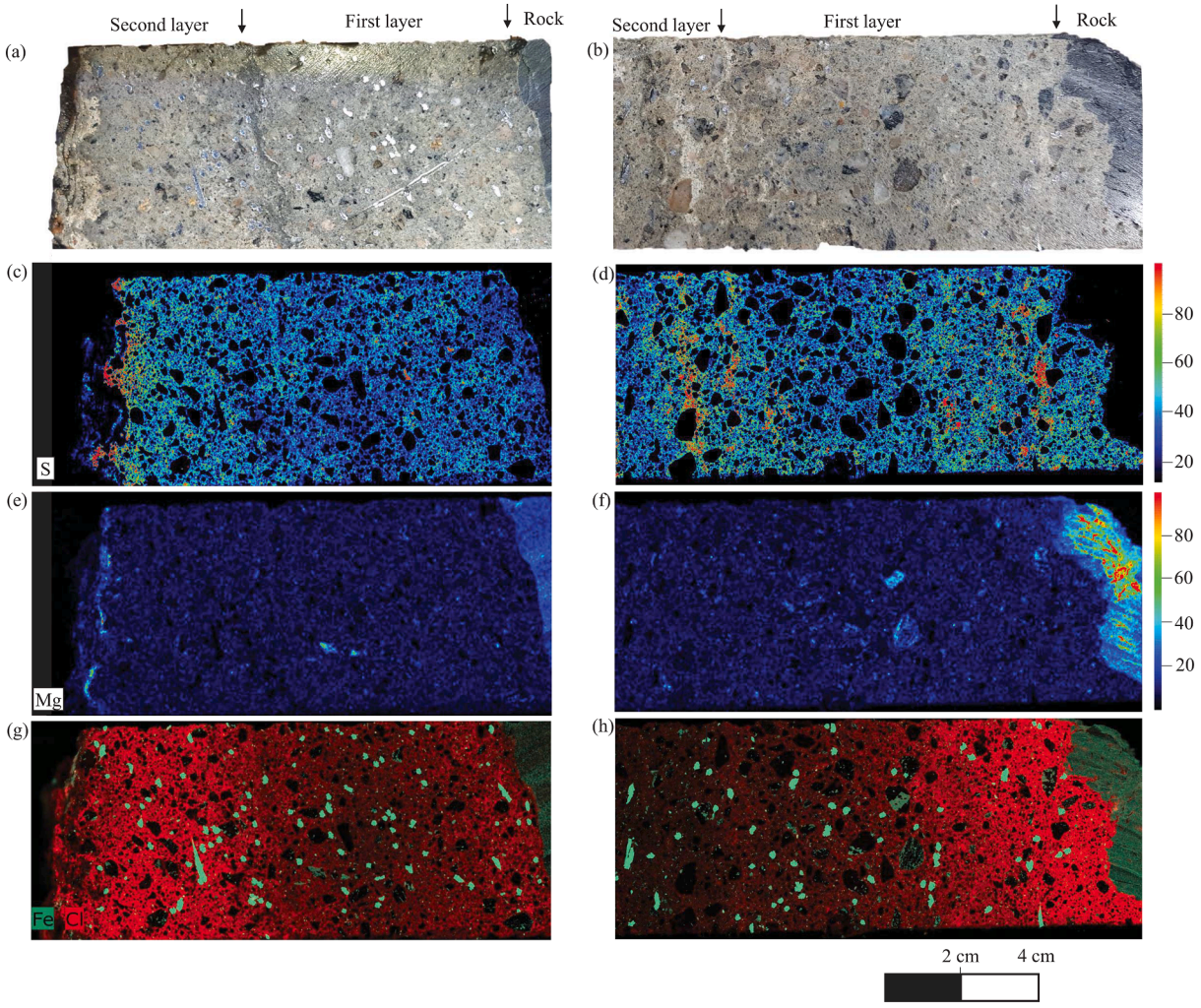

Fig. 12. μ-XRF analysis in cores 2 (on the left) and 14 (on the right) scanned in the same run: (a, b) Real image of one half of the shotcrete core split lengthwise, (c, d) sulfur mapping, (e, f) magnesium mapping, and (g, h) chlorine-iron mapping.

$$V = \frac{W_2 - W_2^{'}}{\rho_w} \tag{2}$$

Where ρ_w is the density of water considered to be 1000 kg/m^3. On the other hand, the volume of the cylindrical samples used for the UCS test is determined by a digital caliper following the standards suggested by the ISRM [43]. Eq. (3) shows the formula used:.

$$V = \frac{\pi^* d^2}{4}^* L \tag{3}$$

Where d and L are the averaged diameter and length dimensions respectively of a shotcrete sample after it has been sliced and ground.

3. Results

3.1. pH indicator

Shotcrete samples from two different cores were tested with the pH indicator Thymolphthalein. The samples chosen for this test belong to the core-end exposed to the traffic room. Fig. 8 shows shotcrete samples from cores 5 and 9 before and after Thymolphthalein is sprayed on them.

Fig. 8 shows that the carbonation depth in zone 1 is slightly higher than in zone 2, exceeding two cm in the first case after approximately 23 years of exposure. It is important to highlight that Fig. 8 suggests that there is no need to spray a pH indicator to determine the carbonation zone since this area stands out for a brownish color, contrasting the gray color of the cement paste. Finally, thanks to the blueish background given by the thymolphthalein in Fig. 8a on the right, some steel fibers can be identified without any sign of corrosion in the uncarbonated zone.

3.2. μ-XRF scanning

Figs. 9-10 show the results of μ-XRF analysis in core 3 (extracted from zone 1) and core 14 (extracted from zone 2) respectively. In the latter case, the μ-XRF scanning is trimmed since the length of the core exceeds the scan range of the machine. The scan length adopted is approximately 16 cm, long enough to include all the shotcrete joints of this core. The rest of core 14 is shown in Fig. 12. Figs. 9-10 are comparable since they were scanned in the same run.

Fig. 9b and Fig. 10b show a higher sulfur content in the cement paste near the traffic room, suggesting that the main source of sulfur comes from the traffic room. However, it is important to highlight that there is a sudden drop in sulfur compounds at the carbonation zone in both cases. Fig. 10b also illustrates sulfur enrichment in shotcrete joints. To a minor extent, Fig. 9b shows sulfur enrichment as well in the shotcrete joint.

With regard to magnesium content along the cores, Fig. 10c does not give any indication of magnesium attack. On the other hand, Fig. 9c shows magnesium enrichment in the cement paste at the far-end of core 3 near the traffic room. If Fig. 9c and Fig. 9d are analyzed together, one

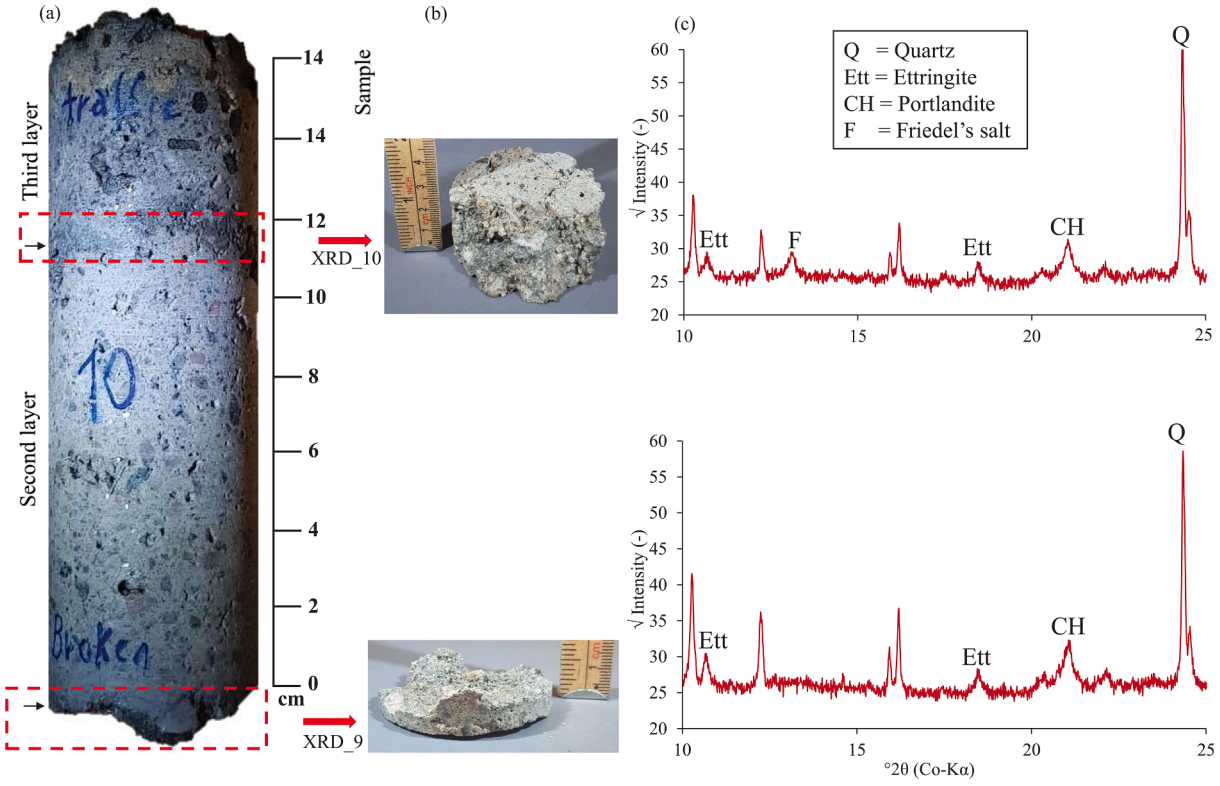

Fig. 13. XRD analyses in shotcrete joints belonging to core 10 from the Nordkapp tunnel where alkali-free accelerator was used. (a) whole shotcrete core, (b) bulk shotcrete joint sample, and (c) XRD results with the square root of the counts in Y-axis.

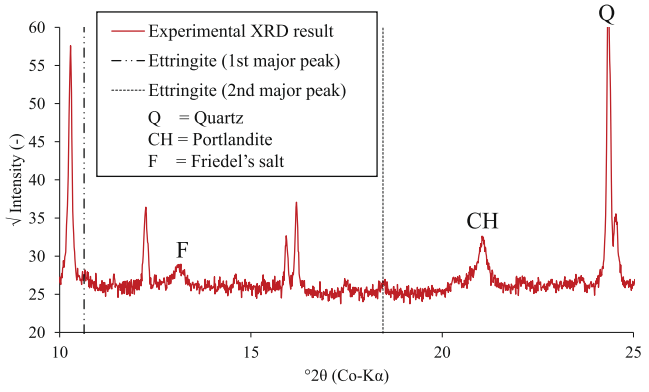

Fig. 14. XRD analysis in bulk shotcrete near the rock obtained from core 13 in the Nordkapp tunnel where alkali-free accelerator was used.

can see that chlorine and magnesium do not overlap.

Regarding the origin of chlorine, Fig. 9d indicates that it comes from the traffic room. This is not surprising due to the use of de-icing salts on the route where the Nordkapp tunnel lies. However, Fig. 10d shows very limited chloride ingress in core 14 from the traffic room.

Fig. 11 focuses on the condition of the steel fibers in the shotcrete layer near the traffic room in cores 3 and 14. Apart from the real images near the traffic room in both cores, the iron mapping through μ-XRF is included in this figure to identify corroded and uncorroded steel fibers along with the corresponding chlorine concentration.

Fig. 8 has already described the link between the brownish color near the traffic room and the carbonation zone affected by a lower pH. The additional information provided by Fig. 11 is the connection between some dark reddish spots in the carbonation zone (Fig. 11a and Fig. 11c) and their iron content (Fig. 11b and Fig. 11d respectively). All of the

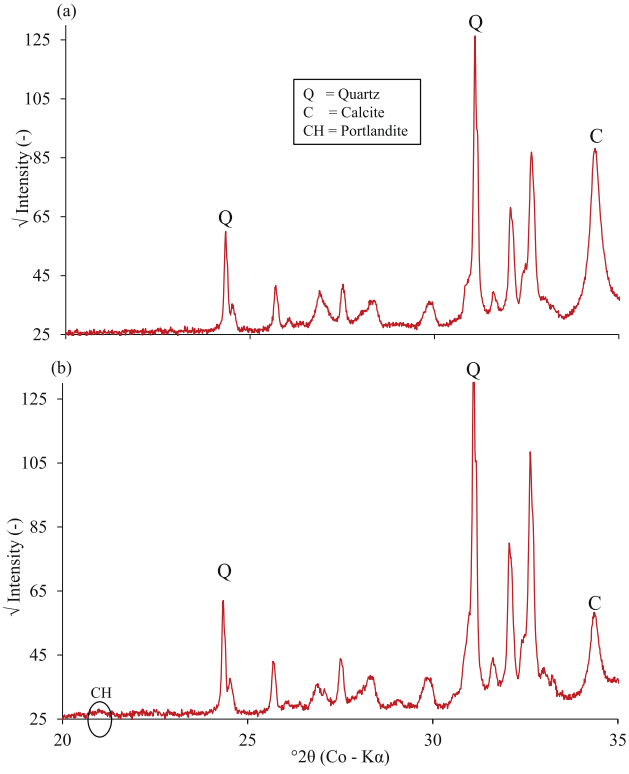

Fig. 15. XRD analyses in shotcrete samples exposed to the traffic room in: (a) Core 4 (zone 1), and (b) core 8 (zone 2).

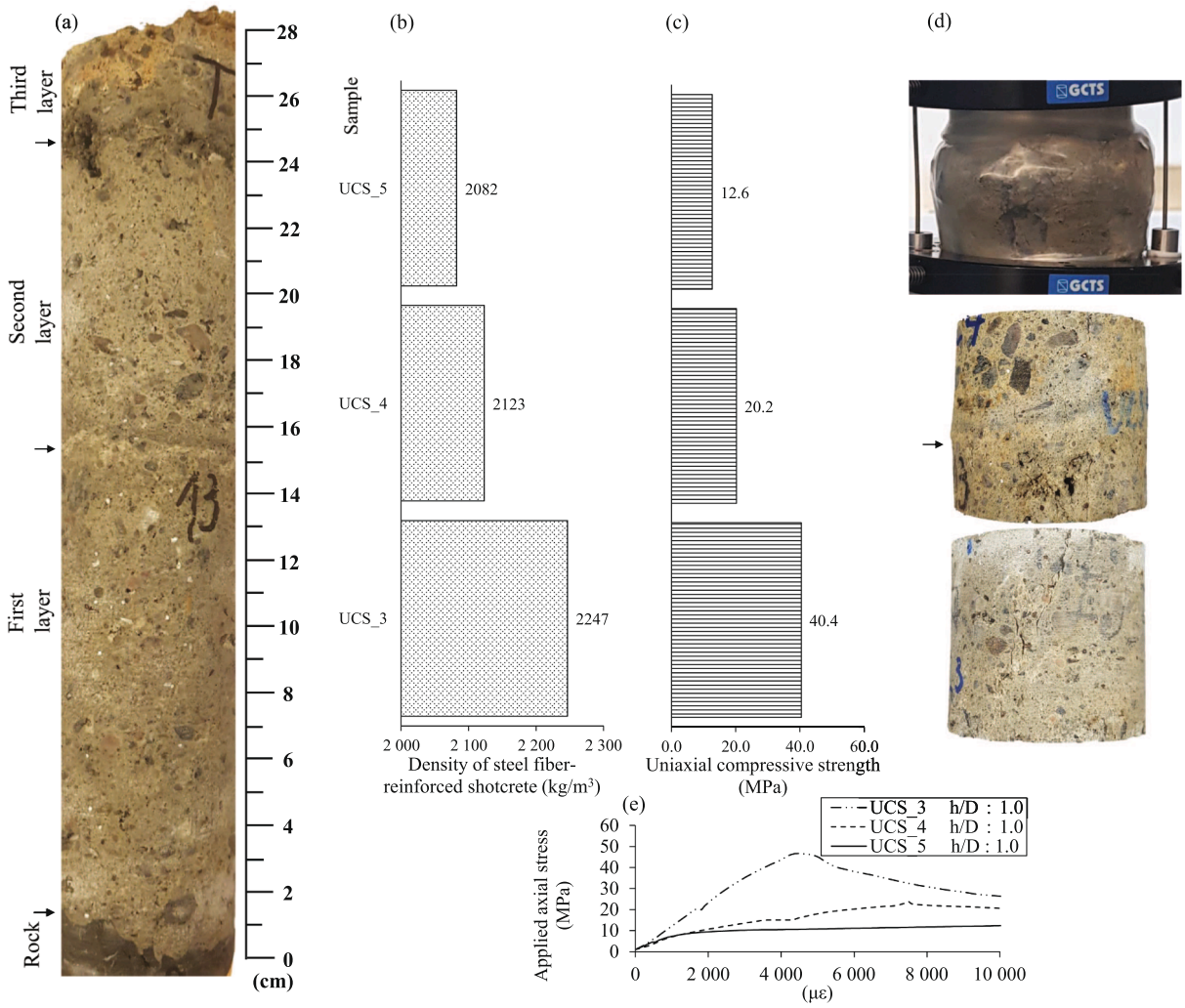

Fig. 16. Core 13 from Nordkapp subsea road tunnel where alkali-free accelerator was used: (a) Whole shotcrete core, (b) density of steel fiber-reinforced shotcrete, (c) equivalent uniaxial compressive test results after applying the correction factors given in Fig. 7, (d) shotcrete sample images after being tested for UCS strength, and (e) stress–strain curve during UCS test with axial deformation.

above strongly suggests that the dark reddish stains are iron oxides, a common corrosion product of steel. Furthermore, note that these dark reddish spots are only identified in the carbonation zone. On the other hand, in the uncarbonated zone steel fibers do not show any sign of corrosion product.

Fig. 9e and Fig. 10e show a similar trend with a reduction in potassium content towards the tunnel room, indicating that alkali-metals in the pore solution are being leached out from the shotcrete layer following the flow direction driven by the hydraulic gradient.

Fig. 12 shows the comparison between the opposite end of core 14 (towards the rock) and core 2.

Alike Fig. 9d, Fig. 12g also illustrates chlorine ingress from the traffic room. These two figures belong to zone 1. What is interesting in both figures is the lower chlorine content in the cement paste near the rock compared to the rest of the shotcrete layer, which suggests that there is no chloride ingress from the rock side. On the other hand, core 14 shows chlorine ingress from the rock (Fig. 12h).

Regarding sulfur intensities comparison between the cores 2, 3 and 14 analyzed through μ-XRF, it is important to mention that the shotcrete joint between the first and second layer in core 14 was mapped twice. The first mapping of this joint was shown in Fig. 10b, which was undertaken in parallel to core 3. The second mapping is shown in Fig. 12d which was simultaneously mapped with core 2. The color difference for the same shotcrete joint in Fig. 10b and Fig. 12d is due to the highest intensity found when mapped. In the first mapping, the highest intensity occurred near the shotcrete surface in core 14 (see Fig. 9b and Fig. 10b as a whole), while in the second mapping similar intensities were found in both the shotcrete joint itself and in core 2 near the shotcrete surface (Fig. 12d and Fig. 12c). Thus, taking as reference this shotcrete joint, it is concluded that the highest sulfur intensity between cores 2, 3 and 14 happened in core 14 (zone 2) near the shotcrete surface adjacent to the carbonation zone.

3.3. XRD

XRD analyses were executed in 12 samples. Emphasis was placed on the core-end towards the traffic room and shotcrete joints. Fig. 13 shows two shotcrete joints belonging to a core extracted from zone 2 where the shotcrete holds alkali-free accelerator.

It is important to highlight that the bulk samples shown in Fig. 13b include aggregates and cement paste. The main peaks with high intensities from the aggregates generally overshadow the intensities of the cement paste. That is why the range of the x-axis in Fig. 13c is only between 10° and 25° and the square root of the intensities were plotted in the Y-axis. The XRD results shown in Fig. 13c detected ettringite in these shotcrete joints. This agrees with Fig. 10b and 12d, where sulfur enrichment was detected in shotcrete joints from a core in the same tunnel zone (zone 2) using μ-XRF.

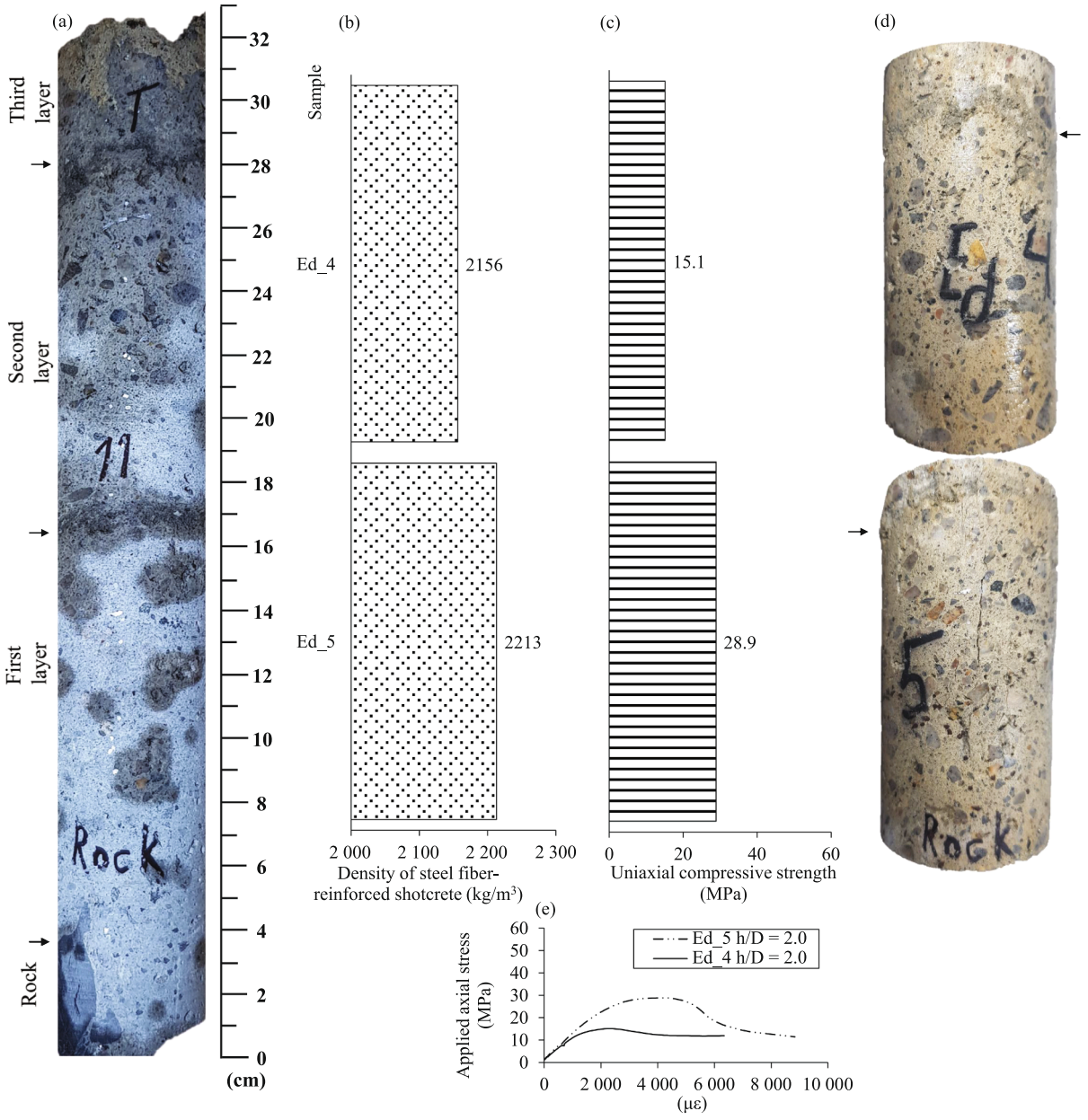

Fig. 17. Core 11 obtained from zone 2 where alkali-free accelerator was used: (a) Whole shotcrete core, (b) density of steel fiber-reinforced shotcrete, (c) uniaxial compressive test results, (d) shotcrete sample images after being tested for UCS strength, and (e) stress–strain curve during UCS test with axial deformation.

When alkali-free accelerator is used, ettringite is expected to be found evenly distributed in the core, and not only in shotcrete joints. An example of a XRD pattern from bulk shotcrete near the rock in the same tunnel zone is showed in Fig. 14. The specimen was obtained from a sample that previously had been used for a UCS test (UCS_3 shown in Fig. 16).

In comparison to the XRD diffraction patterns in Fig. 13, Fig. 14 shows a lower intensity peak for ettringite. In fact, Rietveld analysis performed with the software Topas normalized to 100% crystalline content yields 0.58 % for ettringite in the sample shown in Fig. 14. As a comparison, the Rietveld analyses for the quantification of ettringite in Fig. 13 give 1.66% in sample XRD_10 and 1.08% in sample XRD_9. These results are consistent with the sulfur enrichment detected with μ-XRF and indicate that ettringite enrichment occurs in shotcrete joints where alkali-free accelerator was used.

Friedel's salt mineral was detected between the second and third shotcrete layer of core 10 shown in Fig. 13 (sample XRD_10). Since this shotcrete joint is close to the shotcrete surface, the chlorine element in this mineral came very likely from de-icing salts. In the other shotcrete joint analyzed in this core (sample XRD_9), Friedel's salt was not identified. This second shotcrete joint is approximately in the middle of the total shotcrete layer and probably chloride ingress has not yet reached that far (See Fig. 12h, which is a core located approximately 25 cm apart from core 10 with the absence of chlorine between the first and second shotcrete layer).

Fig. 15 shows a comparison of XRD results in shotcrete samples exposed to the traffic room.

Fig. 15 shows that calcite has formed in the shotcrete exposed to the traffic room. More in detail, Fig. 16b shows that XRD analysis in core 8 (zone 2) still detects portlandite minerals near the shotcrete surface exposed to the traffic room, while the XRD result in core 4 (zone 1) represented in Fig. 16a does not identify portlandite. On the other hand, the latter figure shows a higher intensity for calcite in comparison to Fig. 16b.

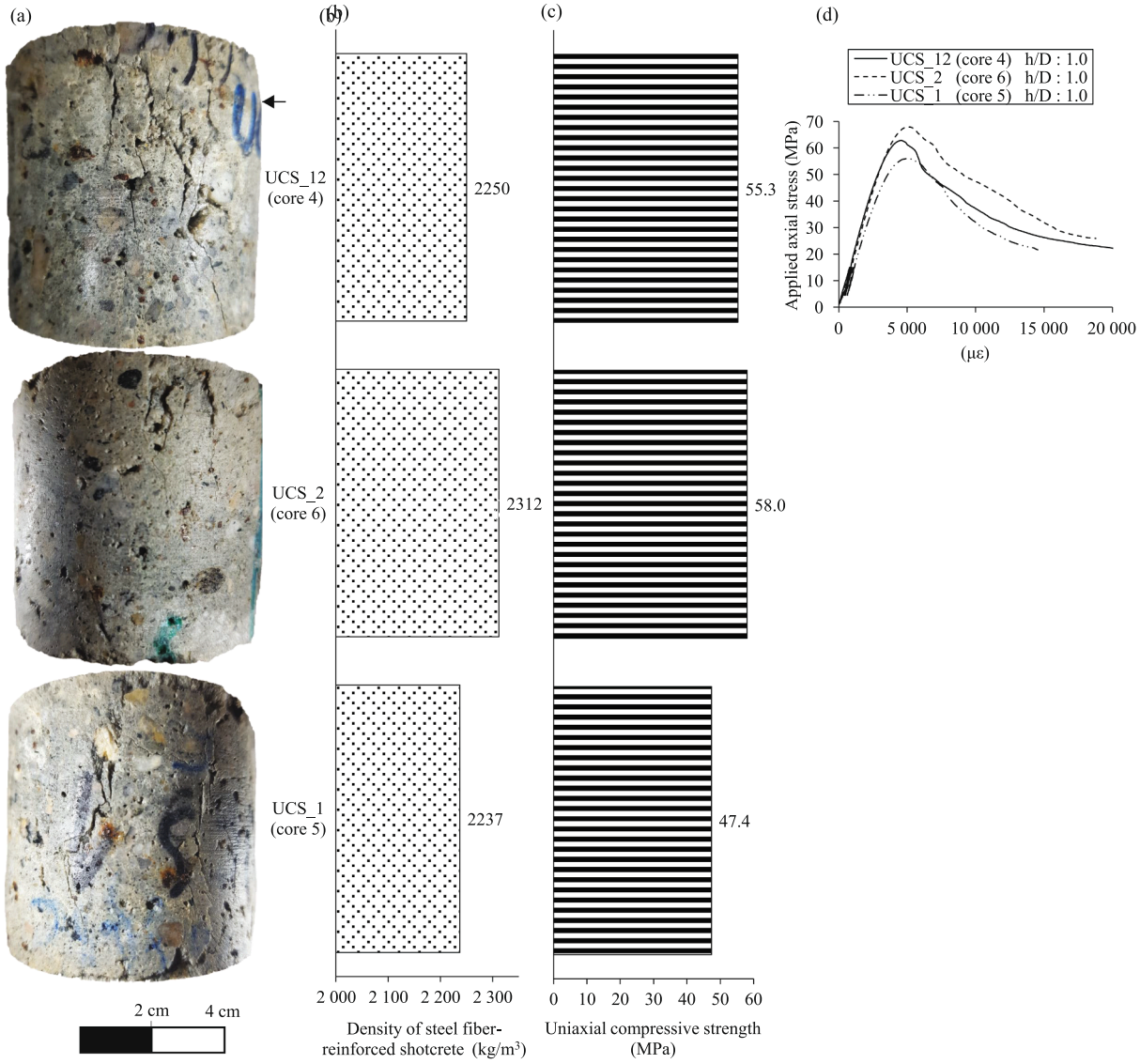

Fig. 18. Three UCS test results obtained from zone 1 where water glass accelerator was used: (a) Shotcrete sample images after being tested for UCS strength, (b) density of steel fiber-reinforced shotcrete, (c) equivalent uniaxial compressive test results after applying the correction factors given in Fig. 7, and (d) stress–strain curve during UCS test with axial deformation.

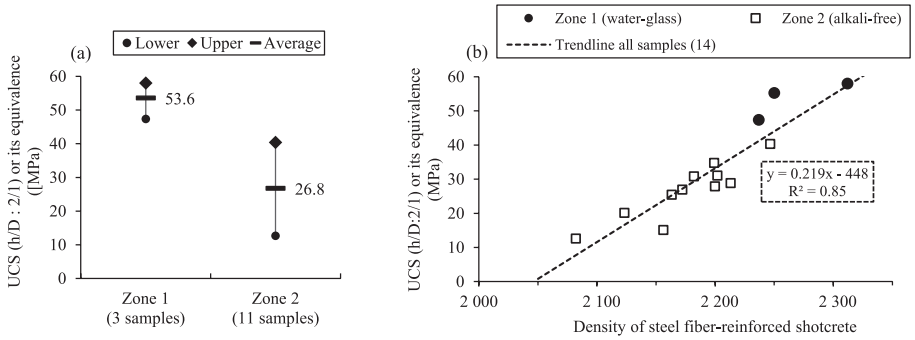

Fig. 19. Statistical analysis related to UCS test results: (a) UCS test results grouped by the tunnel zones where shotcrete cores were extracted, and (b) correlation between UCS test results and shotcrete density broken down for each zone.

Ettringite is only stable when the pH is greater than 10.7 [44]. Then, it is not surprising that the carbonated shotcrete samples exposed to the traffic room shown in Fig. 15 did not detect ettringite, since the carbonation area has a pH below 10.5, as demonstrated by the pH indicator. In agreement with this observation, Fig. 9b and 10b show a sudden reduction in sulfur content in the carbonation zone.

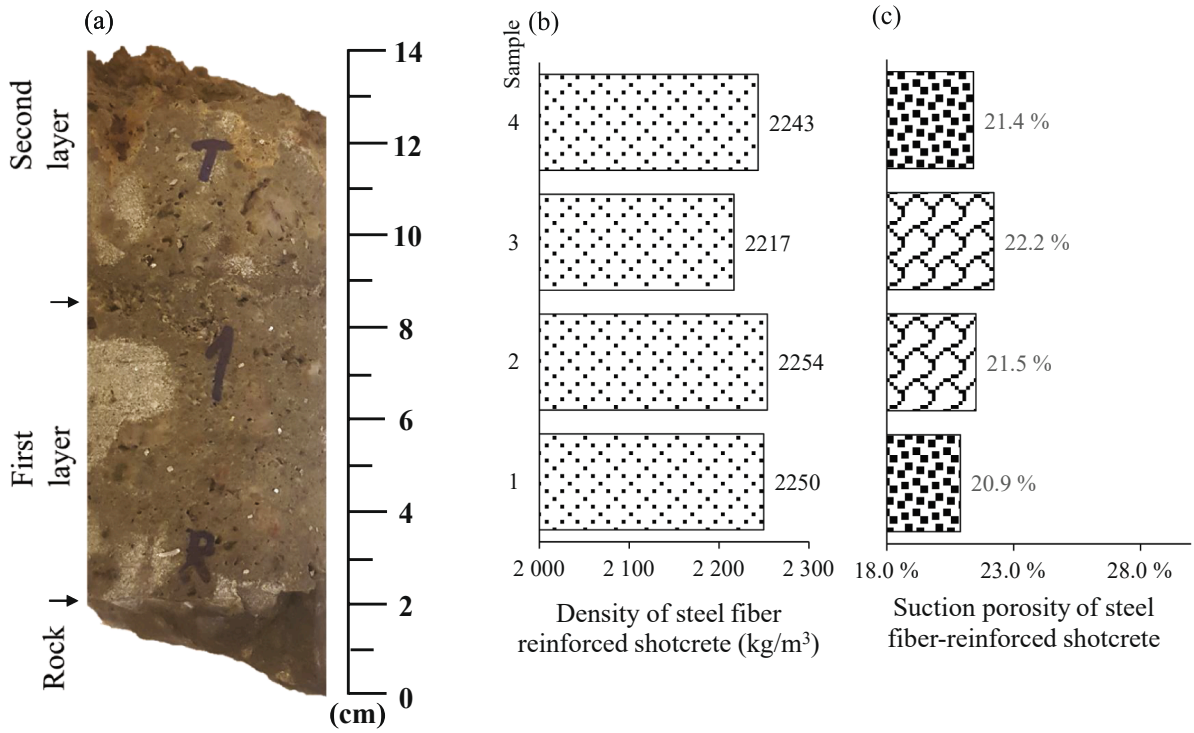

Fig. 20. Core 1 obtained from the Nordkapp tunnel where water–glass accelerator was used: (a) Whole shotcrete core, (b) density of steel fiber-reinforced shotcrete, (c) suction porosity results.

At the carbonation zone, it is reported that Friedel's salt dissolves [24]. Fig. 15 supports this statement where Friedel's salt was not identified in any of the two spectra.

3.4. UCS and density

Since shotcrete samples were weighed before the execution of the UCS tests, it is possible to visualize the relation between the UCS test and shotcrete density results along the cores. Fig. 16 shows the results in core 13 (zone 2 in Table 2).

Fig. 16 clearly shows a decay of.UCS strength towards the traffic room. As a reference, the valid regulations for subsea tunnels in 1996 in Norway required a minimum characteristic compressive strength of a 15 cm cube at 28 days equal to 45 MPa or C45 [45] following the European standards. For strength class C45, the Norwegian guidelines for shotcrete at that time suggested a minimum in-situ strength from extracted core cylinders after 28 days of 28.8 MPa [46]. Then, it is possible to say that sample UCS_3 in Fig. 16 still complies with the original regulations. On the other hand, the strength of sample UCS_5 shows a reduction to approximately 40% of the original compressive strength required.

Fig. 16 also shows that shotcrete density diminishes towards the traffic room in approximately the same proportion as the compressive strength. The stress–strain curve shown in Fig. 16e also indicates a change from a strain-softening behavior near the rock to an elastic–-plastic behavior near the traffic room. In other words, it shows a gradual reduction in the difference between peak and residual values towards the traffic room.

The arrows in Fig. 16a indicate the boundary between two consecutive shotcrete layers. The middle and upper shotcrete samples in Fig. 16 (samples UCS_4 and UCS_5) hold one of these shotcrete joints. Specifically in sample UCS_4, the image after the execution of this UCS test indicates that the shotcrete joint had an influence on the failure mode undergone in this sample. In the case of sample UCS_5, a more extensive degradation is observed which involves the whole sample.

The UCS test results from a core in the same zone (Core 11) is shown in Fig. 17.

Unlike the shotcrete samples shown in Fig. 16, the samples in Fig. 17 have a height-to-diameter ratio equal to two, allowing to determine the UCS strength result without any correction factor. Despite this difference, Fig. 17 shows the same trend as described in Fig. 16 for the UCS test and shotcrete density results.

Due to the thinner total shotcrete thickness in zone 1, a profile of UCS test results along a core in this tunnel zone is not possible to be elaborated. Nevertheless, results of UCS tests from three different cores are shown in Fig. 18.

Fig. 18 shows high shotcrete density values and high UCS strength results in zone 1. This is also the case for sample UCS_12 which held a shotcrete joint. In addition, stress–strain curves show evident differences between peak and residual values. Finally, a statistical comparison of UCS test results between zones 1 and 2 is given in Fig. 19.

Fig. 19a shows that zone 1 has no indication of degradation since it shows high UCS strength values with little scattering. On the other hand, zone 2 shows lower UCS strength values with high scattering.

Fig. 19b incorporates shotcrete density results measured just before the execution of the 14 shotcrete samples tested for UCS strength. This figure clearly illustrates that the highest two UCS test and shotcrete density results correspond to zone 1 and the lowest ten UCS test and shotcrete density results belong to zone 2. It is also important to highlight the good correlation between UCS and shotcrete density test results shown in Fig. 19b, even for extreme values. This is remarkable considering that only some of these samples are shotcrete-joint free and different failure modes took place along with different stress rate applied during testing (strain controlled tests).

3.5. Suction porosity and density

Figs. 20-21 show the results of suction porosity and density along two shotcrete cores extracted in zone 1.

In Fig. 20, samples 2–3 contain shotcrete joints. In Fig. 21, only

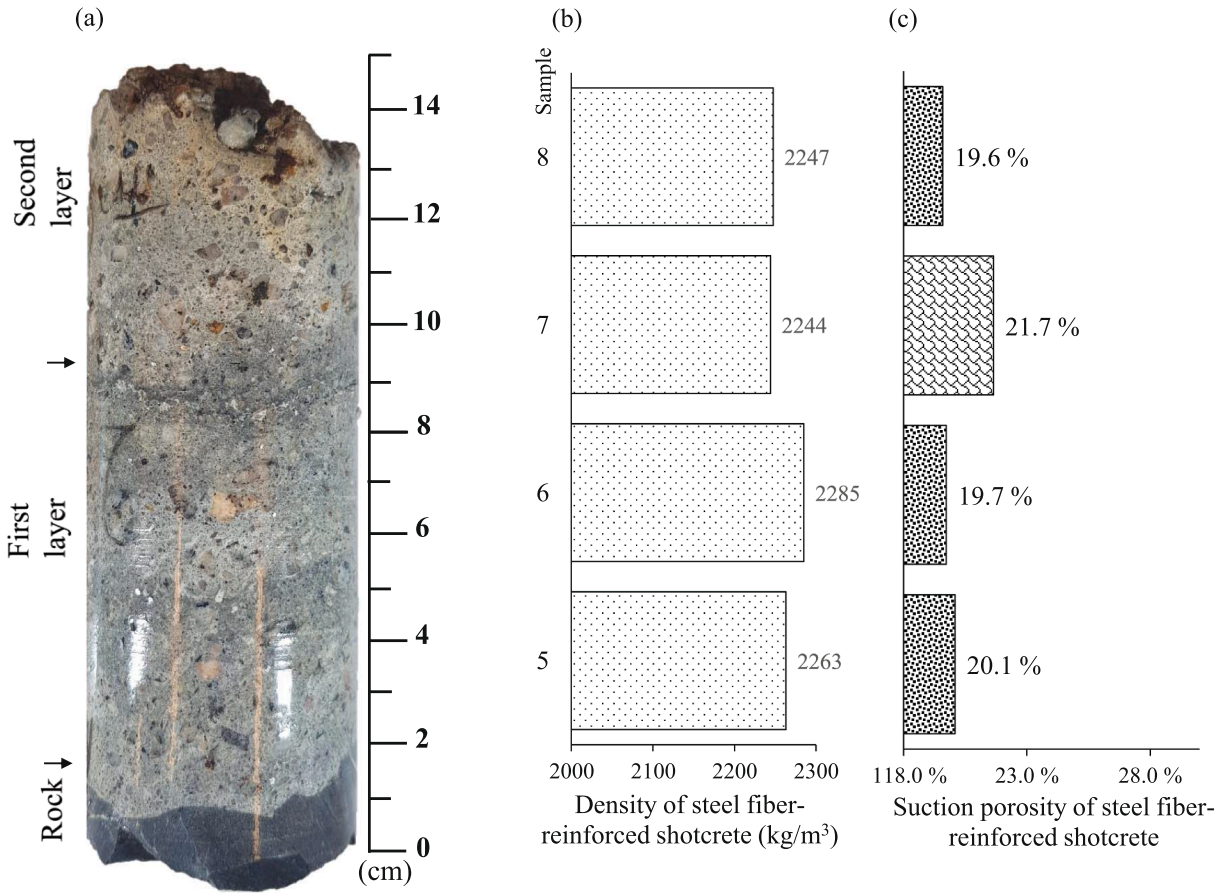

Fig. 21. Core 2 obtained from the Nordkapp tunnel where water–glass accelerator was used: (a) Whole shotcrete core, (b) density of steel fiber-reinforced shotcrete, (c) suction porosity of steel fiber-reinforced shotcrete.

sample 7 holds a shotcrete joint. Figs. 20 and 21 show that shotcrete samples holding shotcrete joints have the highest suction porosity and the lowest shotcrete density in the core.

Fig. 20 shows a slight trend of higher suction porosity towards the traffic room. The exception is the last sample exposed to the traffic room with a sudden decay in suction porosity. This latter observation is probably associated with the formation of calcite in the carbonation zone.

Fig. 22 shows the results of suction porosity and shotcrete density in core 12 (Zone 2).

Fig. 22 shows a clear trend of higher suction porosity and lower shotcrete density towards the traffic room. Alike Figs. 20-21, the samples holding shotcrete joints in Fig. 22 (samples 17 and 20) have the highest suction porosity and lowest density values in the core. In addition, Fig. 22 also indicates carbonation at the far end of the core exposed to the traffic room with a drop in suction porosity.

Fig. 23 shows the results of core 7 located in zone 2 as well.

Fig. 23 shows that the core broke at a shotcrete joint, despite the machine continued drilling for about 10 cm more. In addition, the core in Fig. 23 also gives the highest suction porosity and the lowest density values in the shotcrete joint. The trend in suction porosity and shotcrete density towards the traffic room are similar to Fig. 23. The only exception is sample 10 in Fig. 23 with a local higher density and lower suction porosity.

Finally, a statistical overview of suction porosity results and their relation to shotcrete density are given in Fig. 24 for both tunnel zones.

In comparison to zone 1 in Fig. 24a, zone 2 presents a higher average suction porosity value and a higher dispersion of the results. Both observations indicate that the level of degradation is higher in zone 2.

It is important to point out as well in Fig. 24b the good correlation between suction porosity and shotcrete density test results, even for the extreme values.

4. Discussion

4.1. Sampling and investigation methods

With regard to sample height for UCS tests, traditional concrete testing recommends a nominal h/D of 2 for cylinders [40]. This is a challenging requirement when it comes to shotcrete testing. First of all, the contact between the rock and shotcrete is uneven. The same happens on the shotcrete surface exposed to the traffic room. Then, to get a cylinder of shotcrete with flat surfaces on both ends, the core extracted from the field should have a clearance in length of several cm on top of the required height. In addition, about 5 mm is lost each time the sample is sliced (thickness of diamond saw). This is why, shorter samples with a h/D of 1 were executed in addition to some samples with a h/D of 2. As shown in Fig. 7, the ultimate axial stress obtained with these shorter samples is, in average, 15% higher than those longer ones with a h/D of 2. Alike Fig. 19b, Fig. 25 plots UCS strength results over shotcrete density. However, Fig. 25 groups the samples by h/D instead of the zone where they were extracted.

Fig. 25 illustrates that taller samples (h/D = 2.0) tend to average the results, but all the samples can be linked to the same trend line. When it comes to the analysis of degradation, a test which is more sensitive is valuable, and that is what a shorter sample can give in addition to the creation of profiles along the cores.

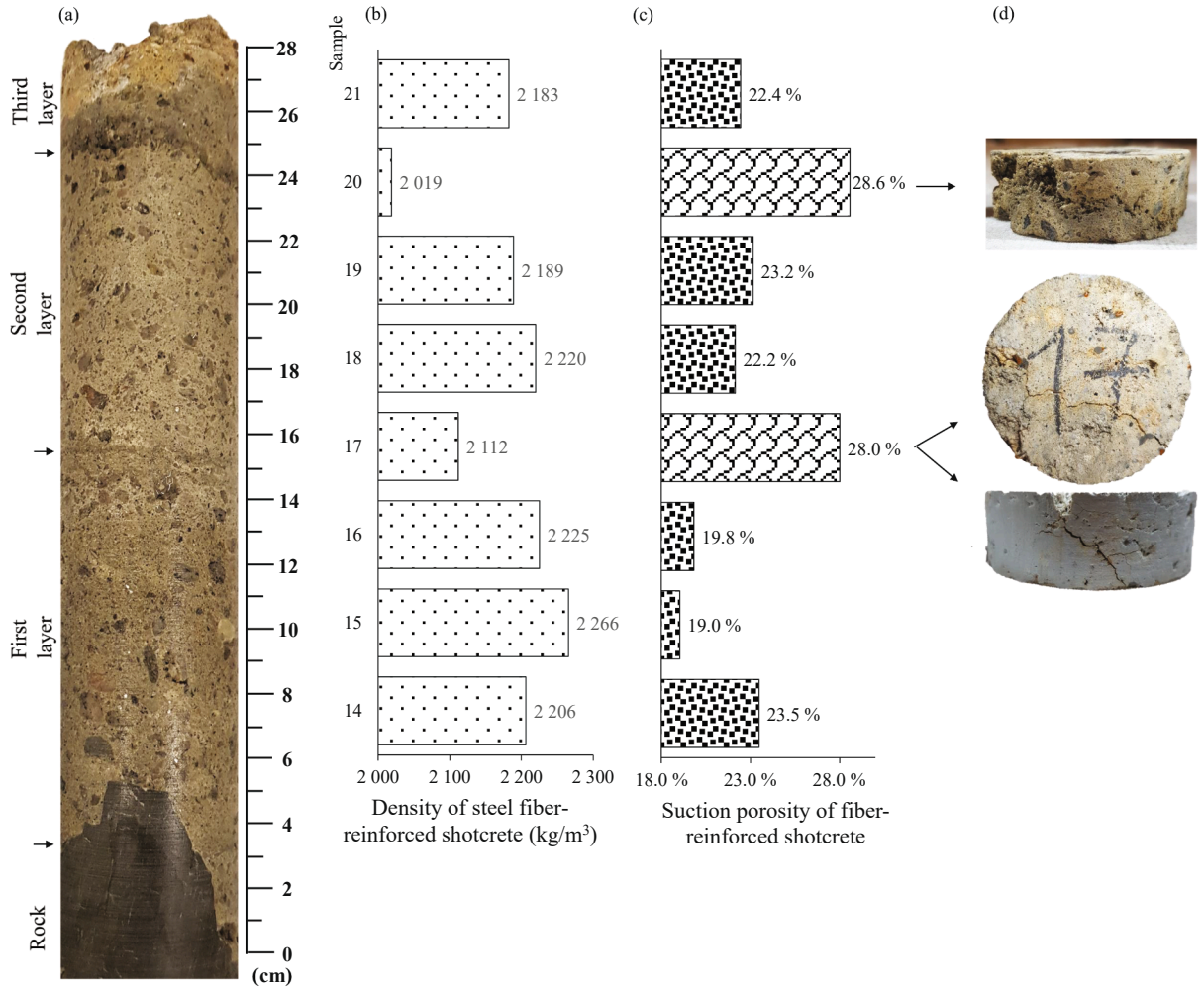

Fig. 22. Core 12 obtained from Nordkapp tunnel where alkali-free accelerator was used: (a) Whole shotcrete core, (b) density of steel fiber-reinforced shotcrete, (c) suction porosity results, and (d) picture of samples holding shotcrete joints at the end of suction porosity test.

4.2. Results

The zones investigated in the Nordkapp tunnel indicate that the in-situ condition of shotcrete with water–glass accelerator (zone 1) is better than the shotcrete installed in zone 2, where alkali-free accelerator was used. This is supported by higher UCS and shotcrete density results along with lower suction porosity values with limited scattering in all the just-mentioned parameters in zone 1.

The observation that the shotcrete with water–glass based accelerator results in a higher long-term strength compared to the one using alkali-free accelerator might be considered in contradiction with several studies reported in the literature. In some studies, however, the comparison of concrete strength with different accelerator types are judged to be unfair, using the highest accelerator dosages in concrete samples containing the water–glass accelerator [29,47]. In these two references, the doses of water–glass accelerator were 10% and 12% respectively, well above the Norwegian practice 25 years ago.

Other studies conclude that alkali-free accelerators are able to reach higher long-term mechanical strength for the shotcrete and reduce the susceptibility to sulfate attack in comparison to alkaline activators [6,25,26,48]. However, in these references, the alkaline accelerators are only represented by sodium aluminate solutions, not sodium silicates (water–glass). In particular, it is concluded that the aluminates are responsible for a higher amount of different aluminate hydrates, among others, monosulfoaluminate. The higher amount of monosulfoaluminate in this type of accelerator makes the concrete more susceptible to form ettringite under an external source of sulfate and inhibits further hydration of the alite at early stages of hydration.

A historic review of shotcrete as rock support in Norway in the mid-1990 s, where water–glass was the dominant accelerator type, concluded that a compressive strength close to 50 MPa from drilled cores after 28 days of curing was normal [49]. Furthermore, another research undertaken in Norway some years later between shotcrete using water–glass and alkali-free accelerators obtained no significant differences in UCS values after 28 days of curing, exceeding the samples 50 MPa regardless of the accelerator type [50]. The main finding of this research is not the satisfactory condition of the shotcrete with water–glass accelerator, but rather the physical and mechanical changes observed in the shotcrete layer where alkali-free accelerator was used.

The leaching severity in zone 2 is observed by:.

- A noticeable decay of density towards the traffic room shown in Figs. 16, 17 and 22
- A significant increase of suction porosity towards the traffic room in Figs. 22-23
- A clear reduction of UCS strength towards the traffic room shown in Figs. 16 and 17

Ettringite enrichment in shotcrete joints is also observed in the shotcrete where the alkali-free accelerator was used. The high suction porosity values measured in these shotcrete joints suggest that there might be a link between the ettringite formation in these joints and the

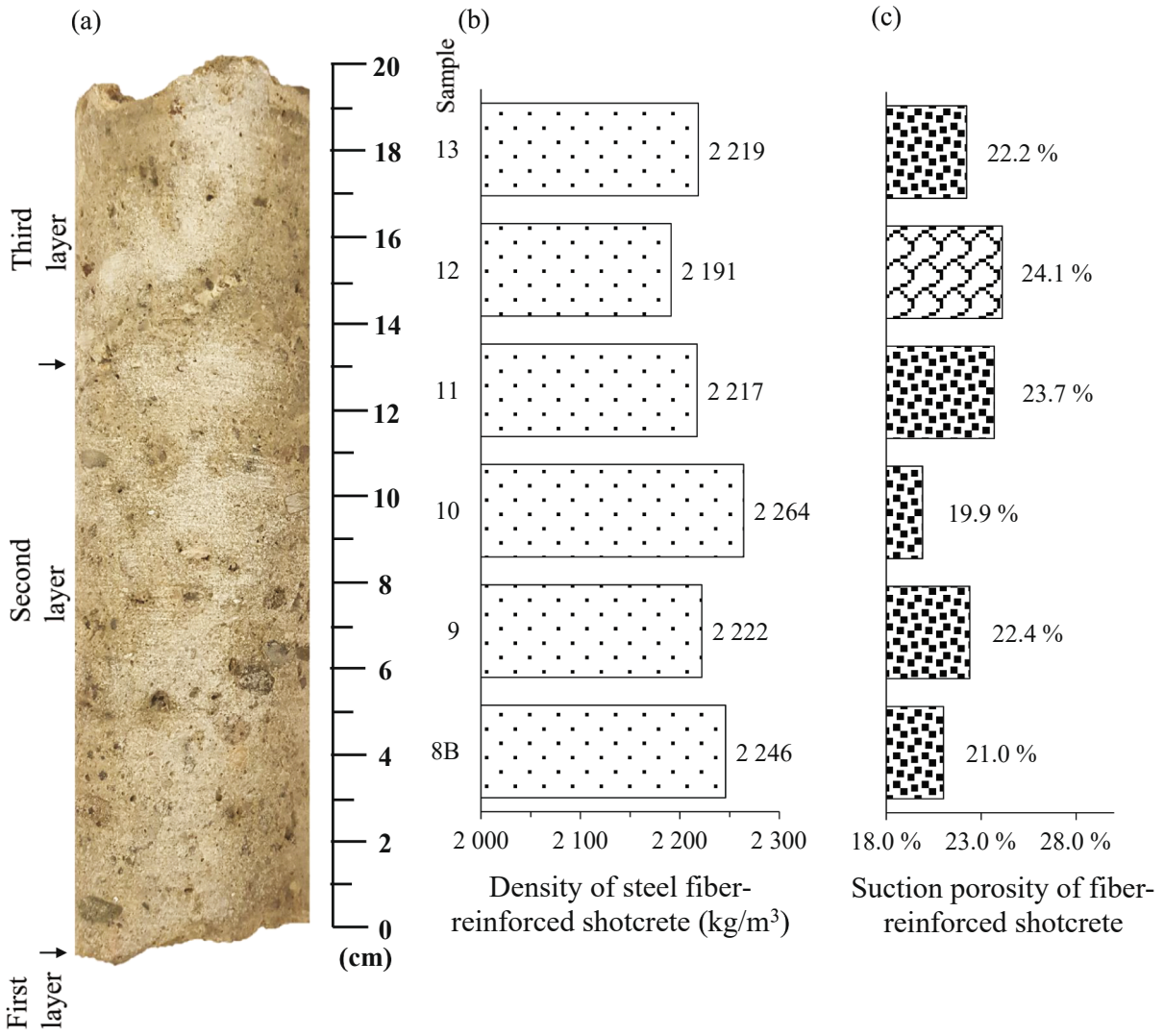

Fig. 23. Core 7 obtained from the Nordkapp tunnel where alkali-free accelerator was used: (a) Whole shotcrete core, (b) density of steel fiber-reinforced shotcrete, (c) suction porosity results.

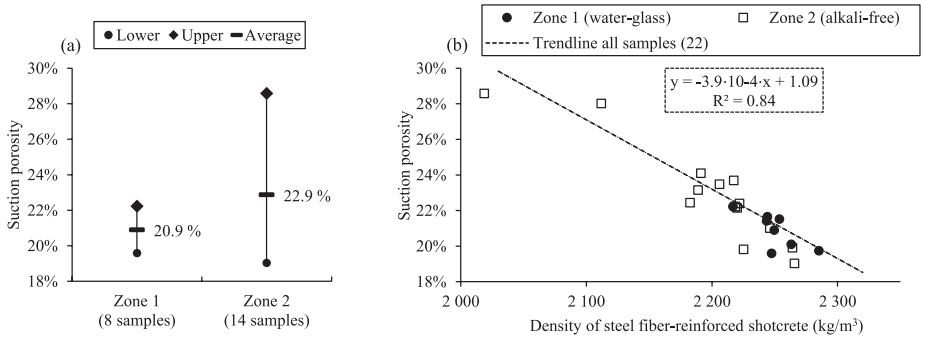

Fig. 24. Statistical analysis related to suction porosity test results: (a) suction porosity results grouped by the zones where shotcrete cores were extracted (See Table 2), and (b) correlation between suction porosity and shotcrete density broken down for the different zones.

eventual increase of suction porosity due to the expansion capacity of ettringite. In this regard, it is important to highlight that sample 17 in Fig. 22, cracked after a drying and wetting cycle for the suction porosity test. This was observed only in this sample out of 22 suction porosity samples. In agreement with these observations, Table 2 indicates that the only two cores which broke at shotcrete joints occurred in cores belonging to zone 2.

The shotcrete condition in zone 2 is poor with a shotcrete joint near the shotcrete surface. In the area of the shotcrete layer just next to the carbonation zone, apart from a higher suction porosity and lower shotcrete density detected, the highest sulfur concentration was observed. Within the carbonation zone, high sulfur concentrations are

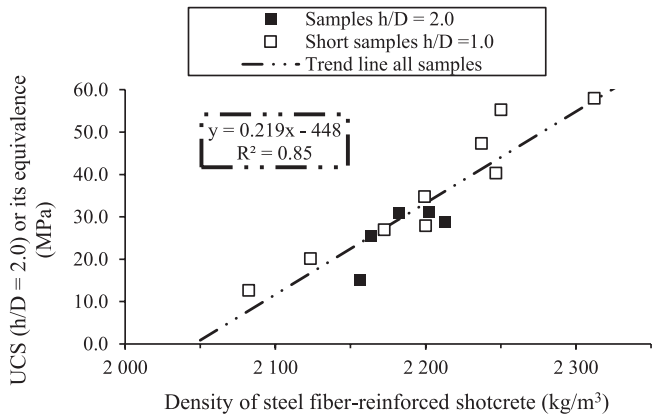

Fig. 25. UCS strength results over density of steel fiber-reinforced shotcrete after immersing the samples in water for seven days. Samples with height-to-diameter ratio of 1 were corrected by Fig. 7.

not expected since several sulfur containing minerals in the cement paste are not stable when the Ph less than 10.7 [44].

Regarding the distribution of sulfur concentration, it is important to mention that to a minor extent zone 1 also contained higher sulfur intensities near the shotcrete surface adjoining the carbonation zone (see Fig. 9b and Fig. 12c). This observation identified in both tunnel zones suggests that there is an extra source of sulfur coming from the traffic room. Thus, the shotcrete with alkali-free based accelerator installed in a subsea road tunnel has three potential sources of sulfur. From the accelerator itself, from the marine groundwater and from the traffic room. With regard to the latter case, air pollution analysis in traffic tunnels describes sulfur dioxide SO_2 as a common gas emitted by vehicles [51,52], which is soluble in water. This is the probable explanation for what was observed near the traffic room in the three cores where μ-XRF analysis was executed.

The sources of sulfur combined with a hydraulic gradient that might promote leaching can create an aggressive interaction for the shotcrete. The availability of Ca, Al and Si ions in the pore solution generated by the leaching of hydrated cement phases facilitate the formation of secondary expansive minerals under an external source of sulfate [18,22]. On the other hand, the higher is the porosity in the concrete caused by leaching, the easier is for aggressive ions to penetrate farther into the concrete. In turn, the cracking generated by sulfate attack can also promote further ingress of aggressive ions in the concrete and promote leaching.

Considering that a higher water-cement ratio leads to a higher suction porosity [53], there is an indication that during construction the water conditions between zones 1 and 2 were different based on the local suction porosity measured near the rock in these two zones. While suction porosity results near the rock in zone 1 were 20.1% and 20.9% (samples 1 and 5 in Figs. 20-21 respectively), the suction porosity measurement near the rock in zone 2 gave 23.5% (sample 14 in Fig. 22). In connection with these findings, there was no sulfur and chlorine ingress from the rock in zone 1 (Fig. 9b and Fig. 12c for sulfur and Fig. 9d and Fig. 12g for chlorine), while there was sulfur and chlorine ingress in zone 2 (Fig. 12d for sulfur and Fig. 12h for chlorine).

Magnesium was identified by μ-XRF analysis near the shotcrete surface exposed to the traffic room in cores 3 and 2 extracted from zone 1 (Fig. 9c and Fig. 12e respectively). None of the XRD analyses in the area identified brucite. The origin of the magnesium content coming from the traffic room is unknown. A possible source of magnesium could be $MgCl_2$ used as dicing salts. However, there is no evidence from the

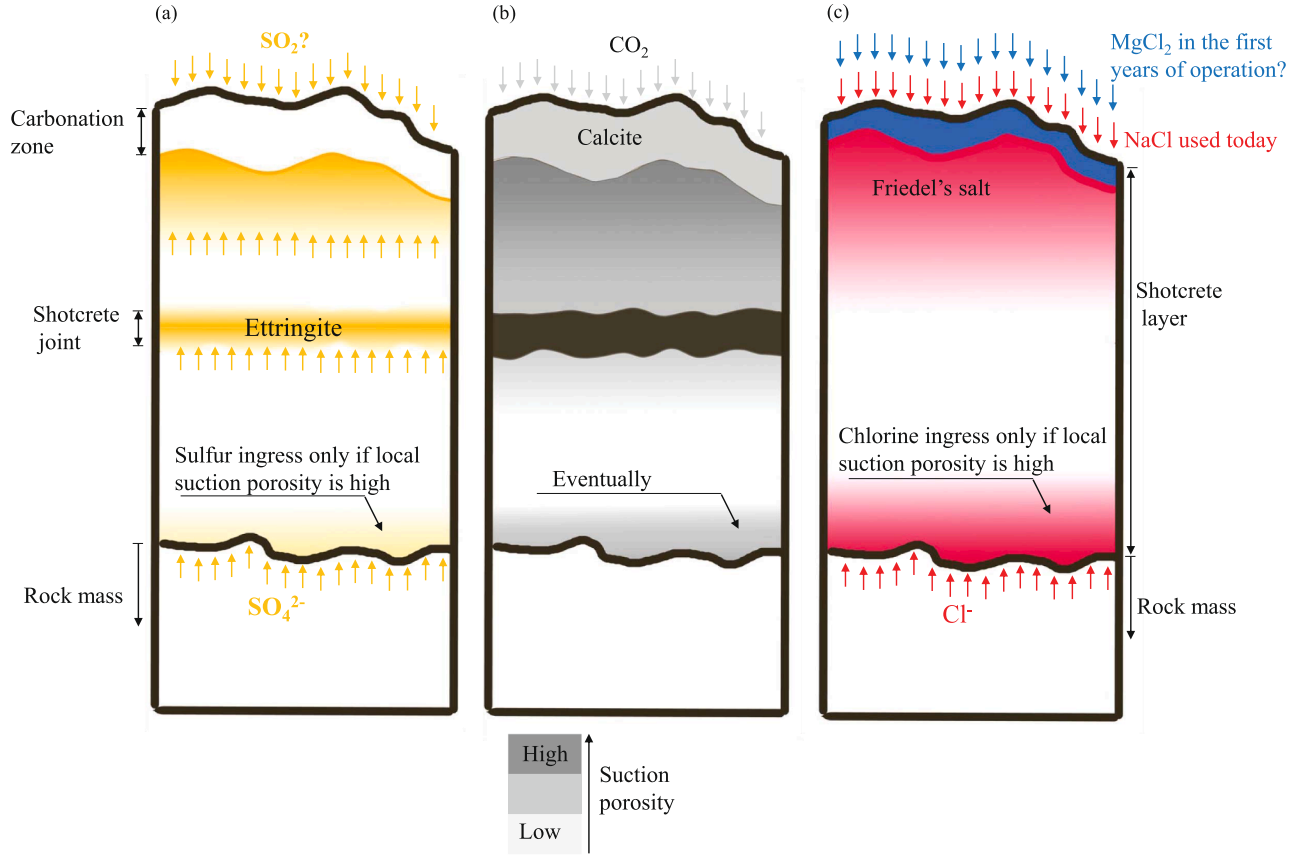

Fig. 26. Summary of observations in the Nordkapp subsea road tunnel. (a) Sulfur ingress and distribution along the core, (b) suction porosity distribution along the core, and (c) chlorine and magnesium ingresses.

road authorities in this regard and today only NaCl is being used for winter maintenance of the roads. The source could also come from saline groundwater running down the shotcrete surface, but this second hypothesis does not explain the lack of magnesium in zone 2 (Fig. 10c), where the shotcrete surface is wet.

In the cores extracted from the Nordkapp subsea road tunnel, a summary of what was observed is given in Fig. 26:

Fig. 26a mainly represents the shotcrete where alkali-free accelerator was used. Nevertheless, sulfur ingress from the traffic room and less evident sulfur enrichment in shotcrete joints are also observed in shotcrete where water–glass accelerator was used. Fig. 26b fairly represents all the shotcrete analyzed. Finally, Fig. 26c shows the ingress of chloride and magnesium ions in the cement paste coming from the traffic room, which was mainly observed in the shotcrete where water–glass was used.

In the carbonation area of the different shotcrete samples, corrosion of steel fibers is expected as the pH decreases and steel fibers depassivate. In addition, there is also chloride attack from the traffic room generated by de-icing salts which are dispersed all over the tunnel lining by the vehicles [54]. In the non-carbonated part, steel fibers are not visible corroded (Fig. 11). A possible explanation is that there is no macro-cell corrosion taking place in the fibers (no huge area difference between localized attack and the rest of the steel passivated) as it happens in rebars or rock bolts under a localized attack. Moreover, a recent experimental study concludes that the critical chloride concentration is higher in steel fiber than in steel rebar, being both embedded in concrete [55].

In the Nordkapp tunnel, there is no risk of frost deterioration since it has anti-freezing doors at both ends of the tunnel. These doors only open during winter when a vehicle approaches the tunnel.

5. Conclusions

The Nordkapp subsea road tunnel was investigated in order to explore the in-service condition of steel fiber-reinforced shotcrete used as permanent rock support without any inner lining after more than 20 years of operation. The inspection of this tunnel offers the opportunity to compare the shotcrete applied with both water–glass and alkali-free accelerator types exposed to saline groundwater. This tunnel is of particular interest because it was the first time alkali-free accelerator was used in Norwegian road tunnels.

Two phenomena are observed in the shotcrete analyzed regardless of the core location:.

1. Carbonation occurs at the shotcrete surface exposed to the traffic room detected by calcite deposition in XRD test, lower pH of the pore solution determined by the thymolphthalein pH indicator and a relative reduction in suction porosity. The carbonation depth exceeds 20 mm in specific spots of the Nordkapp tunnel after 23 years in service.
2. The highest suction porosity and the lowest shotcrete density was observed at the boundary of two consecutive layers (shotcrete joints) in a core. This research highlights these areas as weakness zones within the shotcrete core.

In the specific case of shotcrete with alkali-free based accelerator, indications of leaching was observed by:.

1. A significant increase in suction porosity accompanied by a reduction in shotcrete density towards the traffic room.
2. Noticeable strength reduction along the cores towards the traffic room shown by UCS test results down to 40% of the original strength required in one case in the last 10 cm.

Coincidently with these leaching indications, the highest sulfur concentration detected with μ-XRF occurred near the shotcrete surface, adjoining the carbonation zone, where the suction porosity is high.

Furthermore, in this shotcrete with alkali-free accelerator, indications of leaching and sulfate attack were also observed in shotcrete joints by:.

1. Ettringite enrichment found by XRD analyses and sulfur mapping with μ-XRF.
2. How weak these shotcrete joints showed to be during core extraction, being two cores broken (out of eight cores) in these joints, despite the fact that the drilling continued for approximately 10 more cm.
3. Visible cracks in a sample containing a shotcrete joint used for the suction porosity test after the drying and wetting cycle.

To a minor extent, slightly higher sulfur concentration and suction porosity values were also observed in the shotcrete with water–glass based activator near the shotcrete surface just next to the carbonation zone. Nevertheless, no detrimental mechanical consequences for the shotcrete were found.

Regardless of the accelerator type, a reduction in potassium content was observed in the cement paste towards the traffic room, indicating that alkali-metals are being leached out from the shotcrete layer. However, these profiles did not accurately fit with density and suction porosity profiles along the cores.

Corrosion of steel fibers was only observed within the carbonation area. In the uncarbonated area, steel fibers did not show visible signs of corrosion.

The results obtained from the field in this research highlight the need to study together the susceptibly of sulfate attack and leaching, i.e., to perform laboratory tests on shotcrete samples exposed to sulfate bearing solutions under a unilateral pressure. This research also emphasizes the need to monitor the concentration of different gases in road tunnels as environmental factors which influence the durability of materials. In shotcrete, particular emphasis should be placed on sulfur dioxide.

6. Declarations

This research did not receive any specific grant from funding agencies in the public, commercial, or not-for-profit sectors.

7. Consent for publication

All authors read and approved the revised manuscript.

CRediT authorship contribution statement

Cristobal Javier Manquehual: Conceptualization, Methodology, Data curation, Writing – original draft. **Pål Drevland Jakobsen:** Funding acquisition, Supervision, Writing – review & editing. **Karl Gunnar Holter:** Investigation, Writing – review & editing. **Klaartje De Weerdt:** Writing – review & editing, Validation. **Tobias Danner:** Conceptualization, Writing – review & editing. **Amund Bruland:** Project administration, Supervision.

Declaration of Competing Interest

The authors declare that they have no known competing financial interests or personal relationships that could have appeared to influence the work reported in this paper.

References

[1] E. Broch, E. Grøv, K.I. Davik, The inner lining system in Norwegian traffic tunnels, Tunn. Undergr. Sp. Technol. 17 (2002) 305–314, https://doi.org/10.1016/S0886-7798(02)00026-3.

[2] W. Aldrian, A. Thomas, N. Chittenden, K.G. Holter, Permanent Sprayed Concrete Linings, ITA Working Group n°12 and ITAtech (2020).

[3] O.A. Opsahl, Use of wet-process steel-fibrous shotcrete in tunnel linings, in: T. Tapir (Ed.), International Symposium on Low Cost Road Tunnels, Oslo 1984: pp. 305–315.
[4] R. Kompen, Sprayed concrete for concrete repair: Quality requirements and quality follow-up, Norwegian Public Roads Administration, Internal Report No. 1700 (In Norwegian), 1994.
[5] T.A. Melbye, R.H. Dimmock, Modern advances and applications of sprayed concrete, in: International Conference on Engineering Developments, Hobart, Tasmania, Aust. April, 2001. https://doi.org/10.1201/9781003078678-3.
[6] R.P. Salvador, S.H.P. Cavalaro, I. Segura, A.D. Figueiredo, J. Pérez, Early age hydration of cement pastes with alkaline and alkali-free accelerators for sprayed concrete, Constr. Build. Mater. 111 (2016) 386–398, https://doi.org/10.1016/j.conbuildmat.2016.02.101.
[7] NFF. Norwegian Tunnelling Technology, Publication No. 23, Norwegian Tunnelling Society, 2014.
[8] R. Myrdal, Chemical reflections on accelerators for sprayed concrete: Past present and future challenges, in: 6th International Symposium on Sprayed Concrete, Tromsø Norway, 12–15 Sept, 2011.
[9] NS-EN 934–5:2007, Admixtures for concrete, mortar and grout - Part 5: Admixtures for sprayed concrete. Definitions, requirements, conformity, marking and labelling, 2007.
[10] R. Myrdal, Accelerating admixtures for concrete: State of the art, in: Sintef Rep. No. SBF BK A07025, 2007: pp. 1–35. https://www.researchgate.net/publication/288883755_Accelerating_admixtures_for_concrete.
[11] I.D. Hovland, J.P. Holtmon, C. Hauck, FATIMA - Increased Tunnelling Results with Replacement of Fully Casted Lining at the North Cape Tunnel, in: Third International Symposium on Sprayed Concrete - Modern Use of Wet Mix Sprayed Concrete for Underground Support. Gol, Norway. Sept. 26-29, 1999.
[12] C. Manquehual, J. Johansen, P.D. Jakobsen, B. Nilsen, Operation & Maintenance Costs of Subsea Road Tunnels in Norway, in: ITA-AITES World Tunn. Congr. - WTC2020, 2020: pp. 1569–1575.
[13] K. Melby, E. Ovstedal, F.H. Amundsen, G. Ranes, Subsea road tunnels in Norway. Norwegian Public Roads Administration. Report No. 98, 2002.
[14] K.I. Davik, Proper use of sprayed concrete in tunnels. Norwegian Public Roads Administration, Chapter B, subsea tunnels, (In Norwegian), 1997.
[15] I. Galan, A. Baldermann, W. Kusterle, M. Dietzel, F. Mittermayr, Durability of shotcrete for underground support– Review and update, Constr. Build. Mater. 202 (2019) 465–493, https://doi.org/10.1016/j.conbuildmat.2018.12.151.
[16] K.G. Holter, S. Geving, Moisture Transport Through Sprayed Concrete Tunnel Linings, Rock Mech. Rock Eng. 49 (2016) 243–272, https://doi.org/10.1007/s00603-015-0730-1.
[17] K.G. Holter, Loads on sprayed waterproof tunnel linings in jointed hard rock: A study based on Norwegian cases, Rock Mech. Rock Eng. 47 (2014) 1003–1020, https://doi.org/10.1007/s00603-013-0498-0.
[18] F.R. Steindl, I. Galan, A. Baldermann, M. Sakoparnig, L. Briendl, J. Juhart, M. Thumann, M. Dietzel, R. Röck, W. Kusterle, F. Mittermayr, Sulfate durability and leaching behaviour of dry- and wet-mix shotcrete mixes, Cem. Concr. Res. 137 (2020), 106180, https://doi.org/10.1016/j.cemconres.2020.106180.
[19] F.P. Glasser, J. Marchand, E. Samson, Durability of concrete - Degradation phenomena involving detrimental chemical reactions, Cem. Concr. Res. 38 (2008) 226–246, https://doi.org/10.1016/j.cemconres.2007.09.015.
[20] G. Plusquellec, M.R. Geiker, J. Lindgård, K. De Weerdt, Determining the free alkali metal content in concrete – Case study of an ASR-affected dam, Cem. Concr. Res. 105 (2018) 111–125, https://doi.org/10.1016/j.cemconres.2018.01.003.
[21] Y. Wang, C. Shi, Y. Ma, Y. Xiao, Y. Liu, Accelerators for shotcrete – Chemical composition and their effects on hydration, microstructure and properties of cement-based materials, Constr. Build. Mater. 281 (2021), 122557, https://doi.org/10.1016/j.conbuildmat.2021.122557.
[22] R. Ragoug, O.O. Metalssi, F. Barberon, J.M. Torrenti, N. Roussel, L. Divet, J. B. d'Espinose de Lacaillerie, Durability of cement pastes exposed to external sulfate attack and leaching: Physical and chemical aspects, Cem. Concr. Res. 116 (2019) 134–145, https://doi.org/10.1016/j.cemconres.2018.11.006.
[23] K. De Weerdt, Chloride binding in concrete: recent investigations and recognised knowledge gaps: RILEM Robert L'Hermite Medal Paper, Mater Struct. Constr. 54 (2021) (2021) 1–16, https://doi.org/10.1617/s11527-021-01793-9.
[24] M. Sun C. Sun P. Zhang N. Liu Y. Li J. Duan B. Hou Influence of carbonation on chloride binding of mortars made with simulated marine sand Constr. Build. Mater. 303 2021 https://doi.org/https://doi.org/10.1016/j.conbuildmat.2021.124455.
[25] R.P. Salvador, S.H.P. Cavalaro, R. Monte, A.D. Figueiredo, Relation between chemical processes and mechanical properties of sprayed cementitious matrices containing accelerators, Cem. Concr. Compos. 79 (2017) 117–132, https://doi.org/10.1016/j.cemconcomp.2017.02.002.
[26] R.P. Salvador, D.A.S. Rambo, R.M. Bueno, S.R. Lima, A.D. Figueiredo, Influence of accelerator type and dosage on the durability of wet-mixed sprayed concrete against external sulfate attack, Constr. Build. Mater. 239 (2020), 117883, https://doi.org/10.1016/j.conbuildmat.2019.117883.
[27] G. Tjugum, B. Kristiansen, D.A. Juvik, G.O. Johannessen, The future approach of chemicals in practical production of resistant shotcrete with liquid accelerators without Na+ and K+ which enhance the risk of alkali-silica reaction, in: Second International Symposium on Sprayed Concrete - Modern Use of Wet Mix Sprayed Concrete for Underground Support. Gol, Norway. Sept. 23-26, Norwegian Concrete Association, 1996.
[28] C. Maltese, T. Cerulli, C. Pistolesi, D. Salvioni, E.D. Negro, R. Hansen, Alkali free and alkali rich accelerators for shotcrete: Effects on cement Hydration, in: Fourth International Symposium on Sprayed Concrete – Modern. Use of Wet Mixed Sprayed Concrete, Underground Support, 2002, pp. 238–252.
[29] J. Kim J. Ryu R.D. Hooton Evaluation of strength and set behavior of mortar containing shotcrete set accelerators Can. J. Civ. Eng. 35 2008 400 407 https://doi.org//10.1139/L07-115.
[30] S.T. Lee, D.G. Kim, H.S. Jung, Sulfate attack of cement matrix containing inorganic alkali-free accelerator, KSCE J. Civ. Eng. 13 (2009) 49–54, https://doi.org/10.1007/s12205-009-0049-0.
[31] C. Paglia, F. Wombacher, H. Böhni, The influence of alkali-free and alkaline shotcrete accelerators within cement systems: Influence of the temperature on the sulfate attack mechanisms and damage, Cem. Concr. Res. 33 (2003) 387–395, https://doi.org/10.1016/S0008-8846(02)00967-5.
[32] H. Peinado-Guevara, C. Green-Ruíz, J. Herrera-Barrientos, O. Escolero-Fuentes, O. Delgado-Rodríguez, S. Belmonte-Jiménez, M.L. de Guevara, Relationship between chloride concentration and electrical conductivity in groundwater and its estimation from vertical electrical soundings (VESs) in Guasave, Sinaloa, Mexico, Cienc. e Investig. Agrar. 39 (2012) 229–239, https://doi.org/10.4067/S0718-16202012000100020.
[33] Z. Zheng, Y. Fu, K. Liu, R. Xiao, X. Wang, H. Shi, Three-stage vertical distribution of seawater conductivity, Sci. Rep. 8 (2018) 1–10, https://doi.org/10.1038/s41598-018-27931-y.
[34] P. Hagelia, Deterioration mechanisms and durability of sprayed concrete in Norwegian tunnels. NFF Publication No. 17: Underground openings – operations, maintenance and repair., 2008.
[35] NS-EN 206:2013+A1:2016+NA:2017, Concrete: Specification, performance, production and conformity, 2017.
[36] A.B. Revert, K. De Weerdt, K. Hornbostel, M.R. Geiker, Carbonation Characterization of Mortar with Portland Cement and Fly Ash, Comparison of Techniques, Nord. Concr. Fed. 1/2016. Publ. No. 54. (2016).
[37] F.A. Wahid Characterising concrete using micro X-ray fluorescence (μXRF) Department of Civil and Environmental Engineering 2016 Imperial College London.
[38] J. Lindgård, T. Østnor, B. Fournier, Ø. Lindgård, T. Danner, G. Plusquellec, K., De Weerdt, Determining alkali leaching during accelerated ASR performance testing and in field exposed cubes using cold water extraction (CWE) and μxRF, in, MATEC Web Conf. (2018) 1–8, https://doi.org/10.1051/matecconf/201819903004.
[39] Sintef, Internal procedure No. KS 70110. Concrete testing. Capillary suction capacity and porosity, 1996.
[40] NS-EN 12390-1, Testing hardened concrete Part 1: Shape, dimensions and other requirements for specimens and moulds, 2012.
[41] NS 3420, Description texts for building and construction. Special print on concrete structures., Nor. Counc. Build. Stand. (In Norwegian). (1986).
[42] NS-EN 12390-3:, Testing hardened concrete Part 3: Compressive strength of test specimens, 2019.
[43] ISRM, International Society for Rock Mechanics and Rock Engineering. Suggested Methods for Determining Water Content, Porosity, Density, Absorption and Related Properties and Swelling and Slake-Durability Index Properties, 1977.
[44] A. Gabrisová, J. Havlica, S. Sahu, Stability of calcium sulphoaluminate hydrates in water solutions with various pH values, Cem. Concr. Res. 21 (1991) 1023–1027, https://doi.org/10.1016/0008-8846(91)90062-M.
[45] NPRA, Handbook 021: Road Tunnels. Norwegian Public Roads Administration (in Norwegian)., 1992.
[46] NB, Sprayed Concrete for Rock Support, in: Nor. Concr. Assoc. Publ. No. 7, 1993.
[47] H.G. Park, S.K. Sung, C.G. Park, J.P. Won, Influence of a C12A7 mineral-based accelerator on the strength and durability of shotcrete, Cem. Concr. Res. 38 (2008) 379–385, https://doi.org/10.1016/j.cemconres.2007.09.016.
[48] F. Winnefeld, J. Kaufmann, R. Loser, A. Leemann, Influence of shotcrete accelerators on the hydration of cement pastes and their impact on sulfate resistance, Constr. Build. Mater. 266 (2021), 120782, https://doi.org/10.1016/j.conbuildmat.2020.120782.
[49] A. Bakken, E. Holtermann, Steel fibre reinforced shotcrete for temporary and permanent rock support in tunnels, in: N. Gol, . Sept. (Eds.), 2nd International Symposium on Sprayed Concrete - Modern Use of Wet Mix Sprayed Concrete for Underground Support, 1996, pp. 23–26.
[50] I. Storås, B. Bakke, C. Hauck, K.I. Davik, Full-scale testing of alkali-free accelerators with special emphasis on working environment, safety and quality. Third International Symposium on Sprayed Concrete - Modern Use of Wet Mix Sprayed Concrete for Underground Support. Gol, Norway. Sept. 26-29, 1999.
[51] A. Kristensson, C. Johansson, R. Westerholm, E. Swietlicki, L. Gidhagen, U. Wideqvist, V. Vesely, Real-world traffic emission factors of gases and particles measured in a road tunnel in Stockholm, Sweden, Atmos. Environ. 38 (2004) 657–673, https://doi.org/10.1016/j.atmosenv.2003.10.030.
[52] R. De Fre, P. Bruynseraede, J.G. Kretzschmar, Air pollution measurements in traffic tunnels, Environ. Health Perspect. 102 (1994) 31–37, https://doi.org/10.1289/ehp.94102s431.
[53] J. Pae, Y. Zhang, L.H. Poh, J. Moon, Three-dimensional transport properties of mortar with a high water-to-cement ratio using X-ray computed tomography, Constr. Build. Mater. 281 (2021), 122608, https://doi.org/10.1016/j.conbuildmat.2021.122608.
[54] P. Hagelia, Durability development for sprayed concrete as rock support in different tunnel environments. Norwegian Public Roads Administration. Report No. 566., 2018.
[55] J.P. Hwang, M.S. Jung, M. Kim, K.Y. Ann, Corrosion risk of steel fibre in concrete, Constr. Build. Mater. 101 (2015) 239–245, https://doi.org/10.1016/j.conbuildmat.2015.10.072.